Rtt107 cooperates with Rad55 or Slx4 to maintain genome stability in *Saccharomyces cerevisiae*

Joshua A. R. Brown[1] and Michael S. Kobor[2*]

[1]Centre for Molecular Medicine and Therapeutics, BC Children's Hospital Research Institute, Department of Medical Genetics, University of British Columbia, Vancouver, British Columbia, Canada, V5Z 4H4

[2]Centre for Molecular Medicine and Therapeutics, Edwin S.H. Leong Centre for Healthy Aging, Department of Medical Genetics, University of British Columbia, Vancouver, British Columbia, Canada, V5Z 4H4

*Corresponding author: Michael S. Kobor
msk@cmmt.ubc.ca

Short title: Rtt107, Rad55, and Genome Maintenance

Abstract

A range of genome maintenance factors respond to endogenous and exogenous DNA damage to prevent mutations and cell death. The scaffold protein, Rtt107, is important for the growth of cells exposed to DNA-damaging agents in the budding yeast *Saccharomyces cerevisiae*. Rtt107 binds to a diverse array of partner proteins, such as Slx4, and responds to DNA damage by localizing to phosphorylated histone H2A. Rad55–Rad57, a heterodimer involved in DNA repair, also binds to Rtt107, but the function of the Rtt107–Rad55–Rad57 complex remains unclear. In addition to their sensitivity to DNA-damaging agents, *rtt107*Δ mutants exhibit spontaneous genome instability phenotypes, including spontaneous loss of heterozygosity (LOH) caused by crossovers and other genetic events. However, the binding partners with which Rtt107 interacts to prevent spontaneous genome instability have yet to be elucidated. Here, we showed that Rtt107 acts in the same pathway as Rad55 to limit LOH, specifically by preventing crossover events. A *rad55-S404A* phosphorylation site mutation largely disrupted the interaction between Rtt107 and Rad55–Rad57, resulting in increased LOH and crossover rates, consistent with the contribution of Rtt107–Rad55–Rad57 interaction to genome stability. Strikingly, an *rtt107-K887M* mutation that reduces Rtt107 recruitment to H2A did not result in an LOH phenotype, suggesting that the role of Rtt107 in preventing LOH is distinct from its function as an H2A-binding scaffold. Rtt107 did not function primarily in the same pathway as Rad55 to limit recombination at the sensitive ribosomal DNA (rDNA) locus, but instead acted with Slx4 to maintain rDNA stability, suggesting that interactions of Rtt107 with different partners prevented distinct types of instability. Taken together, our observations suggested that Rtt107 limits spontaneous LOH and crossover events in part by binding to Rad55 in a manner dependent on Rad55-S404.

Author Summary

Numerous proteins are involved in the repair of damaged DNA and prevention of genome instability in cells, which would otherwise result in persistent changes to DNA. Genome maintenance pathways are evolutionarily conserved, and the budding yeast, *Saccharomyces cerevisiae*, is a powerful model organism for investigating the maintenance of genome integrity. Rtt107 is a scaffold protein expressed in yeast, containing conserved protein domains that are important for the function of genome maintenance proteins. Although the functions of Rtt107 in cells treated with DNA-damaging agents have been characterized in some detail, it remains unclear how Rtt107 prevents spontaneous genome instability in cells growing under normal conditions. Here, we found that Rtt107 prevents specific types of spontaneous genome instability and acts in the same pathway as the DNA repair protein, Rad55, to which it binds. Mutation of a possible Rtt107 binding site on Rad55 showed that Rtt107 indeed limited genome instability in part by binding to Rad55. Strikingly, Rtt107 also showed Rad55-independent roles in preventing ribosomal DNA (rDNA) instability, and in this context Rtt107 cooperated in part with its binding partner Slx4. Taken together, our results revealed the pathways by which the evolutionarily conserved protein Rtt107 limits spontaneous genome instability.

57 **1 Introduction**

58 The genome is constantly under threat by a variety of endogenous and exogenous factors,
59 which are counteracted by the DNA damage response (DDR) consisting of interconnected
60 pathways that detect, signal, and repair DNA damage [1,2]. These DDR proteins play crucial
61 roles in ultimately preventing cell death when DNA damage occurs. Genome instability,
62 encompassing both mutations and genomic rearrangements, can also occur as a byproduct of
63 DNA damage and repair. Cells therefore rely on a variety of genome maintenance factors, with
64 functions in the DDR and in processes such as DNA replication, to both survive DNA damage
65 and limit genome instability.

66 DNA double-strand breaks (DSBs) are among the most deleterious types of DNA
67 damage, and can cause cell death if left unrepaired [3]. DSBs and DSB repair can result in a
68 range of types of genome instability, including deletions, gross chromosomal rearrangements
69 (GCRs), and loss of heterozygosity (LOH) [2,3]. DSBs are repaired by a number of different
70 pathways depending on the stage of the cell cycle at which they occur and the nature of specific
71 lesions. In the budding yeast, *Saccharomyces cerevisiae*, DSB repair most frequently involves
72 the homologous recombination (HR) pathway, while non-homologous end-joining (NHEJ) of
73 DSB ends is specifically upregulated in G_1 phase haploid yeast and is the predominant pathway
74 in mammals [4]. HR occurs after resection, the 5′→3′ nucleolytic digestion of DSB ends that
75 exposes single-stranded DNA (ssDNA) and leads to formation of a Rad51–ssDNA filament, and
76 can generate reciprocal crossovers (RCOs) [3]. Alongside specific repair processes, DNA
77 damage prompts a broader DDR that involves checkpoint signaling, which arrests the cell cycle
78 while DNA damage is repaired [5]. Here, histone H2A-S129 phosphorylation (γH2A) is placed
79 by the Mec1 and Tel1 sensor kinases around lesions, and forms a platform for the recruitment of

80 other DDR factors, including checkpoint proteins [6]. Another histone mark, H4T80
81 phosphorylation, is placed near sites of DNA damage by Cla4, although the functional
82 consequences of this chromatin mark in the DDR have yet to be fully elucidated [7].
83 Rtt107 is an evolutionarily conserved protein that plays multiple roles in the DDR, and is
84 required for normal cell growth during chronic exposure to DNA-damaging agents [8]. At the
85 molecular level, Rtt107 localizes to stalled replication forks, DSBs, and other DNA damage
86 sites, where it acts as a scaffold to recruit other proteins to these lesions [9–14]. Rtt107 promotes
87 recovery from treatments that damage DNA and the restart of DNA replication after damage
88 repair, at least in part by limiting DNA damage and preventing checkpoint hyperactivation
89 [8,15–17]. Rtt107 contains six BRCA1 C-terminal (BRCT) domains, which generally mediate
90 both phosphorylation-dependent and -independent protein–protein interactions [8,18], and
91 localizes near DSBs by binding γH2A via BRCT5/6 [10,19]. Rtt107 is also recruited near DSBs
92 by binding phosphorylated H4T80 via BRCT1–4, with this representing the first identified
93 molecular interaction partner of phosphorylated H4T80 [7]. The interaction of Rtt107 with γH2A
94 is mediated by Rtt107-K887 and is required for its localization near DSBs [10,19], whereas
95 interaction with phosphorylated H4T80 is mediated by Rtt107-K426 and partially contributes to
96 its localization near DSBs [7]. Both *rtt107-K426A* and *rtt107-K887M* mutants exhibit
97 hypersensitivity to chronic treatment with DNA-damaging agents, suggesting that Rtt107 confers
98 DNA damage resistance, at least in part, by localizing to histone marks [10]. Rtt107–BRCT1–4
99 forms a tetrahedral structure that binds a variety of complexes, and in turn Rtt107 may act as a
100 scaffold by recruiting these partners to γH2A-containing regions, to which Rtt107 itself is
101 tethered via BRCT5/6 [9,14,15,20].
102

103 Rtt107 has been studied most extensively in the context of its localization to γH2A and
104 its constitutive interaction with the Slx4 endonuclease [10,14,15]. DNA damage induces
105 interaction of the Rtt107–Slx4 complex with the replication factor, Dpb11 [21]. In turn, this
106 Rtt107– Slx4–Dpb11 interaction can competitively reduce the interaction between Dpb11 and
107 the checkpoint factor, Rad9, while increased Rad9–Dpb11 interaction in the absence of the
108 Rtt107–Slx4 complex can limit DSB resection and may contribute to checkpoint hyperactivation
109 [16,17,22–24]. Slx4 is also required for phosphorylation of the SQ/TQ motifs of Rtt107 by Mec1
110 after treatment with the DNA-damaging agent, methyl methanesulfonate (MMS) [8,15].
111 However, it is unclear which functions of Rtt107 are dependent on its phosphorylation [8,21,25].
112 Rtt107 interacts with the Rad55–Rad57 heterodimer via Rtt107–BRCT1–4, and Rad55
113 contains an Rtt107 interaction motif that was shown to interact with Rtt107–BRCT1–4 *in vitro*
114 [14,20]. However, the molecular function of the Rtt107–Rad55–Rad57 complex has yet to be
115 determined. In general, Rad55–Rad57 acts as a recombination mediator, which promotes Rad51–
116 ssDNA filament assembly for HR [26–30]. In contrast to the *rtt107*Δ mutant [8], both *rad55*Δ
117 and *rad57*Δ mutants are sensitive to treatment with ionizing radiation [27,31], which induces
118 DSBs. These findings suggest that Rtt107 may be less important for successful DSB repair than
119 Rad55–Rad57, or alternatively that the importance of Rtt107 is limited to specific contexts. In
120 addition to promoting DSB repair as a recombination mediator, Rad55–Rad57 also plays a role
121 in DNA damage tolerance pathways that allow DNA lesions to be bypassed during replication
122 and gap filling after replication [32]. Here, Rad55–Rad57 promotes the error-free postreplication
123 repair (PRR) tolerance pathway, also known as template switching, by bridging Rad51 to the Shu
124 complex [33–36]. Recent work also suggested that Rad55–Rad57 may downregulate the
125 translesion synthesis (TLS) pathway [37]. Although *rtt107*Δ mutants exhibit spontaneous Rad52

126 foci [38], a marker of DNA damage and recombination, it has not been determined whether
127 Rtt107 is important for any DNA damage repair function of Rad55–Rad57.

128 The function of Rtt107 in the context of exposure to DNA-damaging agents has been
129 documented in detail, while the role of Rtt107 in preventing spontaneous genome instability is
130 only beginning to be elucidated. Originally, the *rtt107*Δ mutant was identified in screens for
131 mutants with elevated levels of spontaneous LOH and GCRs, chromosomal instability, and
132 phenotypes reflecting spontaneous DNA damage foci and DDR signaling [38–42]. The *rtt107*Δ
133 mutant also exhibits hyperrecombination at the ribosomal DNA (rDNA) locus [38], a highly
134 transcribed series of tandem repeats spanning ~10% of the *S. cerevisiae* genome that represents a
135 unique challenge to the maintenance of genome stability [43]. Taken together, these phenotypes
136 indicate that Rtt107 plays an important role in preventing several types of spontaneous genome
137 instability. However, it remains to be explored whether the role of Rtt107 in preventing
138 spontaneous instability is related to its established functions in the response to exogenous DNA-
139 damaging agents. Rtt107 binds to a variety of DDR complexes in addition to Slx4 and Rad55–
140 Rad57, and it is possible that Rtt107 cooperates with one or several of its documented binding
141 partners to prevent spontaneous genome instability. These partners include the SMC5/6
142 (Structural Maintenance of Chromosomes) complex, Rtt101–Mms1–Mms22, and Mus81–
143 Mms4–Cdc7–Dbf4–Cdc5 [9,12,21,44–46]. Further, Rtt107 was shown to interact with the Sgs1
144 helicase in a yeast two-hybrid screen [20].

145 Genetic interactions underlying genome instability phenotypes represent powerful tools
146 for investigating gene function, and epistatic interactions can often be interpreted in the
147 framework of classical biochemical pathway models [2]. Here, we made use of a comprehensive
148 suite of genetic analyses to uncover the specific pathways in which Rtt107 prevents specific

149 types of spontaneous genome instability. First, we established that the function of Rtt107 in
150 preventing spontaneous LOH was distinct from its role as a γH2A-binding scaffold and from the
151 role of Rtt107 in the context of chronic exposure to DNA-damaging agents, but that Rtt107–
152 BRCT5/6 was still important for preventing spontaneous LOH. Next, we found that Rtt107
153 cooperated specifically with Rad55 to limit LOH as well as mitotic RCO events. A *rad55-S404A*
154 mutant showed reduced interaction between Rtt107 and Rad55 and increased rates of mitotic
155 RCOs and LOH, although the *rtt107*Δ and *rad55-S404A* mutations also made independent
156 contributions to the LOH rate. However, rather than functioning with Rad55 to limit spontaneous
157 recombination at the rDNA locus, Rtt107 cooperated with Slx4 to maintain rDNA stability.
158 Taken together, these results demonstrated that the role of Rtt107 in preventing LOH was largely
159 independent of its previously identified function as a γH2A-binding scaffold, and indicated that
160 Rtt107 cooperated with Rad55 or Slx4 to prevent different types of instability at distinct genetic
161 loci.

162 **2 Materials and Methods**

163 **2.1 Yeast strains and plasmids**

164 Yeast strains used in this study are listed in Table S1, made using standard genetic
165 techniques. The primers used to generate the Rad57-HA construct also encoded a
166 GCAGCAGCAGCAGCAGCAGCA linker between Rad57 and the HA tag (primers available
167 upon request).

168 The plasmids used in this study are listed in Table S2, and were produced using standard
169 genetic techniques. Plasmids pMK429 and pMK430 were generous gifts from Dr. Jocelyn Krebs
170 (University of Alaska Anchorage), and were used in the experiments presented in Figure 2C to
171 examine the *H2A-S129A* allele.

172

173 ## 2.2 Genome instability assays

174 Several assays for genome instability phenotypes were applied in this study under normal
175 growth conditions. Each assay is briefly summarized below and outlined schematically in Fig. 1.

176 ### 2.2.1 Quantitative bimater assay

177 The procedure for the quantitative bimater assay was adapted from a previous report [25].
178 An overnight culture of a *MAT*a mating tester strain was grown in YPD at 30°C, diluted, and
179 plated onto solid medium containing no amino acids (−AA plates). Overnight cultures of the test
180 strain were grown at 30°C and diluted. Cultures were then plated at different dilutions onto −AA
181 plates to count mating events with the *MAT*a tester and onto YPD plates to score total counts.
182 Plates were grown at 30°C for 2–3 days before counting. Mating rates and 95% confidence
183 intervals were calculated with the maximum likelihood estimate method, implemented using the
184 `newton.LD.plating` function in the `rSalvador` R package [47]. Statistical significance
185 was assessed by comparing the overlap of confidence intervals [48], and comparisons between
186 strains were considered significant if the 95% confidence intervals did not overlap. This
187 approach is more stringent than a conventional *p*-value cutoff of 0.05 [48].

188 The bimater assay shown in Figure 2B was adapted to maintain plasmid selection. Strains
189 were grown in SC-Leu medium, and mated to a *leu2*Δ mating tester strain.

190 ### 2.2.2 Reciprocal crossover (RCO) assay

191 RCO events were examined using *can1-100* and *SUP4-o* alleles on chromosome V, as
192 described previously [49]. Independent colonies were grown on YPD plates for 2 days and
193 resuspended in water. Cells were plated at different dilutions onto solid SC-Arg medium with or

194 without 250 μg/mL of canavanine sulfate (Sigma). Plates were grown for 4 days at 30°C and
195 stored at 4°C for 1 day to allow colony color development. Red/white sectored colonies on plates
196 containing canavanine were scored as representative of RCO events in the interval between
197 *CEN5* and *CAN1* loci. Counts were compared to colony counts on plates lacking canavanine, and
198 the frequency of RCOs was calculated. Statistical significance was assessed using Student's *t*
199 test.

200 **2.2.3 Quantitative A-like faker (ALF) assay**

201 A quantitative version of the A-like faker (ALF) assay was performed using the same
202 method as the bimater assay, except that *MATα* haploid strains were examined for their ability to
203 mate with a *MATα* tester strain. Mating rates and statistical significance were calculated using
204 the same methods as described above.

205 **2.2.4 rDNA recombination assay**

206 An rDNA recombination assay was adapted from a previous report to allow for
207 quantification by fluctuation analysis [50]. Strains were plated onto solid medium lacking
208 adenine and grown for 2 days at 30°C. Independent cultures were grown in liquid medium at
209 30°C for 2 days. Diluted cultures were plated onto solid medium lacking arginine with or
210 without 120 μg/mL canavanine (Sigma). Plates with canavanine were incubated for 2 days,
211 replica plated onto media with or without adenine, and incubated for 2 days. Canavanine-
212 resistant colonies that did not grow on plates lacking adenine were scored as representative of
213 rDNA recombination. Scored colonies were compared to colony counts from plates lacking
214 canavanine. The rDNA recombination rates and statistical significance were calculated by the
215 method described for mating rates in the bimater assay.

216 **2.2.5 Diploid instability assay**

217 The assay used to examine various types of genome instability in diploids shown in
218 Figure 6C was adapted from a previous report [49]. Colonies were grown, diluted, and plated as
219 described for the RCO assay. Colonies were plated at separate dilutions to examine Class 5/6
220 events due to their lower rates. After 4 days of growth at 30°C, colonies were replica plated onto
221 several types of solid media to score growth phenotypes, as described previously [49]. Plates
222 were grown at 30°C for 2 days and stored at 4°C for 2 days to allow colony color development.
223 Non-sectored colonies were scored as representative of Class 1–6 events according to their
224 respective growth phenotypes. Mutation rates and statistical significance were calculated as
225 described for mating rates in the bimater assay. A total of 28 Class 3 mutants were examined by
226 PCR as described previously [49] to discriminate between local gene conversion and *de novo*
227 mutation events at the *SUP4-o* locus.
228

229 **2.3 DNA damage sensitivity assays**

230 Overnight cultures grown in YPD at 30°C were diluted to 0.5 OD_{600}. Cells were then 10-
231 fold serially diluted, and plated on YPD medium containing the indicated concentration of MMS,
232 HU, or CPT (Sigma). Plates were incubated for 2 days at 30°C.
233

234 **2.4 TCA extraction**

235 Overnight cultures were diluted to 0.3 OD_{600} in YPD medium and grown to mid-log
236 phase. Whole-cell extracts were prepared by glass bead lysis in the presence of trichloroacetic
237 acid (TCA). Samples were boiled for 5 min and resolved by 8% SDS-PAGE. Western blotting
238 analysis was performed using anti-FLAG M2 (Sigma) and anti-PGK1 (Thermo Fisher)
239 antibodies.

240 **2.5 Analytical-scale protein–protein interaction assay**

241 Overnight cultures were diluted to 0.3 OD_{600} in 4 L of YPD medium, and grown to mid-
242 log phase. The procedure for co-immunoprecipitation was adapted from a previous report [51].
243 Briefly, cells were disrupted with a coffee grinder in the presence of dry ice pellets and
244 resuspended in TAP-IP buffer (50 mM Tris, pH 7.8, 150 mM NaCl, 1.5 mM MgAc, 0.15%
245 Nonidet P-40, 1 mM DTT, 10 mM NaPPi, 5 mM EGTA, 5 mM EDTA, 0.1 mM Na_3VO_4, 5 mM
246 NaF, and Roche cOmplete™ Protease Inhibitor Mix). Crude extracts were prepared by
247 centrifugation, and incubated for 2 hours at 4°C with anti-FLAG M2 antibody (Sigma)-coupled
248 Dynabeads (Invitrogen). Beads were washed with TAP-IP buffer. Captured protein was detected
249 by immunoblotting with anti-FLAG M2 antibody (Sigma) and visualized using an Odyssey
250 Infrared Imaging System (Licor). Co-purifying proteins were imaged with anti-HA (Sigma) and
251 anti-VSV (Bethyl Laboratories) antibodies. Anti-PGK1 (Thermo Fisher) and anti-VSV (Bethyl
252 Laboratories) antibodies were applied to the input fraction as loading controls.

253 **3 Results**

254 **3.1 Rtt107–BRCT1–4 and BRCT5/6 were important for limiting spontaneous LOH**

255 Despite the identification of a number of Rtt107 binding partners and of the molecular
256 functions of Rtt107 in cells exposed to DNA-damaging agents, it remains an important question
257 how Rtt107 operates to prevent a variety of types of spontaneous genome instability. As Rtt107
258 acts as a scaffold by binding to different partners via Rtt107–BRCT1–4 and BRCT5/6, we first
259 examined which structural features of Rtt107 were required for limiting spontaneous genome
260 instability. For this purpose, we examined a spontaneous LOH phenotype that was previously
261 identified for the *rtt107*Δ mutant using the bimater assay (Fig. 1) [25,39]; this assay determines
262 the rate of LOH at the mating type locus in diploid yeast and therefore captures a range of

263 underlying mechanisms, encompassing mitotic recombination, gene conversion, chromosome
264 loss, and chromosomal rearrangements including deletions. We targeted previously studied
265 Rtt107 features with point mutations and a C-terminal truncation (Fig. 2A), and examined the
266 impacts of these mutations on spontaneous LOH rates. The interaction of Rtt107 with γH2A is
267 largely disrupted by the *rtt107-K887M* mutation [10,19], and C-terminal truncation of Rtt107
268 after aa820 (*rtt107*Δ*BRCT5/*6) was used to disrupt any other protein–protein interactions that
269 may require BRCT5/6 [10]. We used the *rtt107-K426M* mutation within BRCT1–4 to disrupt the
270 binding of Rtt107 to phosphorylated H4T80 [7], although it should be noted that Rtt107–
271 BRCT1–4 also has additional binding partners that could be affected by this specific point
272 mutation [9,14,15,20]. We examined other regions of Rtt107 using nonphosphorylatable
273 mutations of each SQ/TQ motif in the SQ/TQ cluster of Rtt107 (*rtt107-4A*) [8], and a mutation
274 designed to disrupt the functions of Rtt107– BRCT1/2 (*rtt107-K192M*) [10]. First, we confirmed
275 that plasmid-borne *RTT107* reduced the rate of LOH in the *rtt107*Δ mutant to close to that seen
276 in wild-type cells (Fig. 2B) consistent with previous reports of a bimater phenotype for the
277 *rtt107*Δ mutant [24,28]. Note that in these experiments, comparisons were considered
278 statistically significant if the 95% confidence intervals did not overlap (see *Materials and*
279 *Methods*). The *rtt107-K887M* mutation did not result in an increase in rate of LOH, suggesting
280 that the function of Rtt107 in this context may be independent of its localization to γH2A. In
281 contrast, the *rtt107*Δ*BRCT5/6* mutation resulted in an elevated LOH rate, similar to complete
282 loss of Rtt107. This suggested that BRCT5/6 played a γH2A-independent role in genome
283 maintenance. The *rtt107-K426M* mutation increased the rate of LOH in this assay, indicating that
284 BRCT1–4 also contributed to LOH prevention. In contrast, the *rtt107-K192M* and *rtt107-4A*
285 mutations did not affect rescue of the bimater phenotype. This was perhaps unsurprising in the

286 case of the *rtt107-K192M* mutation, which has been shown not to disrupt Rtt107 function in
287 other contexts [10]. Taken together, these data indicated that both Rtt107–BRCT1–4 and Rtt107–
288 BRCT5/6 contributed to LOH prevention.

289 We next confirmed that the function of Rtt107 in this context was indeed independent of
290 its localization to γH2A, as our data from the *rtt107-K887M* mutant suggested. For this purpose,
291 we examined whether a nonphosphorylatable *H2A-S129A* mutation affected the ability of Rtt107
292 to limit spontaneous LOH. The results indicated that incorporation of the *H2A-S129A* allele
293 increased the rate of LOH in the bimater assay, consistent with the function of γH2A in the DDR
294 (Fig. 2C) [52]. The *rtt107*Δ mutation increased the rate of LOH of the *H2A-S129A* mutant
295 indicating that Rtt107 and γH2A had independent functions in this context, and that Rtt107 did
296 not prevent spontaneous LOH by acting as a scaffold localized to γH2A.

297 **3.2 Rtt107 acted in the same pathway as Rad55 to limit spontaneous LOH**

298 Having found that multiple domains of Rtt107 contributed to its function in maintaining
299 genome stability but that Rtt107 localization to γH2A was not required, we next examined
300 whether Rtt107 limited genome instability in concert with its known physical interaction
301 partners. We first tested whether the role of Rtt107 in limiting spontaneous genome instability
302 was related to its well-characterized function in downregulating the Rad9–Dpb11 interaction,
303 which has been examined previously in the context of treatment with DNA-damaging agents
304 [16]. To determine whether the genome instability of the *rtt107*Δ mutant was due to increased
305 Rad9–Dpb11 interaction, we utilized a *rad9-ST462,474AA* allele (hereafter referred to as *rad9-*
306 *2A*), which disrupts the Rad9–Dpb11 interaction and partially suppresses the MMS sensitivity of
307 the *rtt107*Δ mutant [17,53]. We compared the *rtt107*Δ, *rad9-2A*, and *rtt107*Δ *rad9-2A* mutant
308 phenotypes in the bimater assay, and found that the *rad9-2A* allele modestly increased the LOH

309 rate compared to the wild-type control (Fig. S1). Introduction of the *rad9-2A* allele into the
310 *rtt107*Δ mutant background increased the rate of LOH to approximately double that of the
311 *rtt107*Δ single mutant, suggesting that spontaneous LOH in the *rtt107*Δ mutant was not caused
312 by Rad9–Dpb11 interaction. It should be noted that strains carrying genomic *H2A/H2B* gene
313 derivatives were used in this assay and subsequent experiments, and the *rtt107*Δ mutation caused
314 a somewhat stronger phenotype in this context compared to strains with plasmid-borne *H2A/H2B*
315 genes (Fig. 2C).

316 As Rtt107 did not prevent spontaneous LOH by regulating the Rad9–Dpb11 interaction
317 or localizing to γH2A, we next examined whether Rtt107 limits genome instability by
318 cooperating with its other known or putative physical interaction partners, specifically Slx4,
319 SMC5/6, Mms22, Mms4, Sgs1, and Rad55 [9,12,21,44–46]. For this purpose, we compared the
320 bimater phenotype of the *rtt107*Δ mutant to strains with mutations of Rtt107 physical interaction
321 partners as well as corresponding double mutants (Fig. 3A–F). Specifically, we sought to identify
322 a mutation in an Rtt107 interaction partner that had a similar spontaneous LOH phenotype to the
323 *rtt107*Δ mutant, and that exhibited epistasis with the *rtt107*Δ mutation. We used a hypomorphic
324 *smc6-9* allele to examine the essential SMC5/6 complex (Fig. 3B) [54], as the *smc6-9* mutant
325 shows a defect similar to the *rtt107*Δ mutant in DSB relocalization to the nuclear periphery [55].
326 We used an *mms4-8A* allele to reduce the interaction between Rtt107 and Mus81–Mms4 (Fig.
327 3D) [45]. Of the mutations examined, only the *rtt107*Δ *rad55*Δ double mutant had a phenotype
328 similar to those of the *rtt107*Δ and *rad55*Δ single mutants, indicating an epistatic interaction
329 between the two mutations (Fig. 3F). This pattern was not observed for mutants of other Rtt107
330 binding partners, and was consistent with an overlap in function between Rtt107 and Rad55 in
331 preventing spontaneous LOH.

332 **3.3 Rtt107 acted in the same pathway as Rad55 to limit spontaneous mitotic RCOs**

333 As the *rtt107*Δ, *rad55*Δ, and *rtt107*Δ *rad55*Δ mutants all exhibited a similar LOH
334 phenotype, we next interrogated the relation between Rtt107 and Rad55 in greater detail. Given
335 the complexities and interrelations between genes involved in the DDR, we first tested whether
336 the relation observed between the *rtt107*Δ and *rad55*Δ mutations was dependent on strain
337 background. Specifically, a *rad5-535* allele is present in the canonical W303 yeast strain
338 background used here, and this can possibly affect findings of DDR studies [56]. To test whether
339 this mutation might affect our results, we repeated the bimater assay in a *RAD5*-corrected W303
340 background. Reassuringly, we observed a similar pattern of LOH phenotypes (Fig. 4A), although
341 perhaps not surprisingly the LOH rates for each strain were much lower than those in the *rad5-*
342 *535* background (Fig. 3F). This indicated that the epistatic interaction between the *rtt107*Δ and
343 *rad55*Δ mutations was not dependent on the presence of the *rad5-535* allele, although LOH rates
344 may be mediated in some way by Rad5, and again suggested that Rtt107 may act in the same
345 pathway as Rad55 to limit spontaneous LOH

346 As a shared function for Rtt107 and Rad55 has not yet been identified, we sought to
347 characterize the degree of cooperation between Rtt107 and Rad55 in limiting spontaneous
348 genome instability in more detail. LOH in the bimater assay is predominantly mediated by
349 crossover events produced by mitotic recombination in wild-type yeast cells [39]. Given that the
350 Rad55–Rad57 heterodimer acts as a mediator of homologous recombination, which can produce
351 mitotic RCO, we hypothesized that spontaneous RCO may occur in the *rtt107*Δ and *rad55*Δ
352 mutants. Therefore, we tested whether Rtt107 and Rad55 limited the rate of spontaneous mitotic
353 RCO, and whether they did so by acting within the same pathway. We examined the *rtt107*Δ and
354 *rad55*Δ mutants by sectoring assay for spontaneous mitotic RCOs within a 120-kb interval on

355 chromosome V in diploid cells, as described previously [49]. It should be noted that this and all
356 subsequent experiments regarding the relation between *RTT107* and *RAD55* were performed in
357 the *RAD5*-corrected W303 background, as described above. The *rtt107*Δ and *rad55*Δ mutants
358 showed higher frequencies of spontaneous RCOs than the wild-type control (Fig. 4B). The
359 *rtt107*Δ single mutant and *rtt107*Δ *rad55*Δ double mutant showed similar increases in mitotic
360 RCO frequency, suggesting that Rtt107 and Rad55 limited RCOs by acting within the same
361 pathway.

362 Next, we tested whether Rtt107 and Rad55 cooperated to limit other genomic events in
363 addition to RCOs that may have caused LOH in the diploid bimater assay, such as gene
364 conversion, chromosomal rearrangements, and chromosome loss. Each of these events, other
365 than RCOs, can be captured by the ALF assay that measures loss of mating locus function in
366 haploid cells [39]. Consistent with an earlier screen, quantitative ALF assay showed that the
367 *rtt107*Δ and *rad55*Δ mutants both exhibited higher mating rates than the wild-type (Fig. 4C) [39].
368 The *rtt107*Δ *rad55*Δ double mutant phenotype trended toward a slightly higher mating rate than
369 either of the single mutants, although the difference was not statistically significant. These
370 observations suggested that Rtt107 and Rad55 may partly act within the same pathway to limit
371 the types of genome instability that are captured by the ALF assay. However, as it remained
372 formally possible that Rtt107 and Rad55 had independent functions in this context, we focused
373 on exploring other genome instability phenotypes.

374 The observations outlined above suggested that Rtt107 cooperated with Rad55 to prevent
375 specific types of genome instability at the mating locus and on chromosome V in diploid cells.
376 Next, to test whether Rtt107 prevented various types of spontaneous instability more broadly at
377 different genetic loci, we examined spontaneous recombination at the sensitive rDNA locus [43].

378 Specifically, we used a quantitative version of an assay for rDNA recombination based on the
379 loss of an *ADE2-CAN1* marker in the rDNA of haploid yeast to monitor rDNA instability [50].
380 The *rtt107*Δ mutant exhibited rDNA hyperrecombination, as reported previously (Fig. 4D) [38].
381 The *rad55*Δ mutant exhibited a modest (~2-fold) increase in spontaneous rDNA recombination,
382 which was significantly less than that in the *rtt107*Δ mutant (~5-fold), suggesting that Rtt107 did
383 not primarily maintain rDNA stability by cooperating with Rad55. Consistent with largely
384 separate roles of Rtt107 and Rad55 in rDNA maintenance, the *rtt107*Δ *rad55*Δ double mutant
385 showed a trend toward greater instability than the *rtt107*Δ single mutant, although this increase
386 was not statistically significant. We considered that Rtt107 may instead maintain rDNA stability
387 with its major binding partner, Slx4, which maintains rDNA structure during DNA replication
388 [57]. Both the *slx4*Δ single mutant and *rtt107*Δ *slx4*Δ double mutant exhibited rDNA
389 hyperrecombination at rates similar to that of the *rtt107*Δ mutant (Fig. S2), which suggested that
390 Rtt107 maintained rDNA stability by cooperating with Slx4 rather than Rad55.
391
392 Our results up to this point supported substantial overlap in function between Rtt107 and
393 Rad55 in preventing specific types of spontaneous genome instability. We next examined the
394 degree of cooperation between Rtt107 and Rad55 during chronic treatment with DNA-damaging
395 agents to clarify the degree of cooperation between Rtt107 and Rad55 in the DDR. Focusing on
396 agents previously shown to cause sensitivity to strains lacking Rtt107, we examined whether
397 Rtt107 and Rad55 acted in the same DDR pathway to confer resistance to the DNA-damaging
398 agents MMS, hydroxyurea (HU), or camptothecin (CPT) in a growth assay (Fig. 4E). Given the
399 extreme sensitivity of the *rad55*Δ mutant to these agents, phenotypic comparison of the *rad55*Δ
400 mutant and *rtt107*Δ *rad55*Δ double mutant required their use at low concentrations. However, it

401 should be noted that the reported sensitivity of the *rtt107*Δ mutant to these agents was not readily
402 apparent at the low concentrations used in this study [8,58]. We first confirmed that the *rtt107*Δ
403 *rad55*Δ mutant exhibited enhanced MMS sensitivity compared to single mutants, as reported
404 previously [20]. Next, we found that the *rad55*Δ mutant exhibited much greater sensitivity to HU
405 and CPT than the *rtt107*Δ mutant. The *rtt107*Δ *rad55*Δ double mutant also showed similar HU
406 sensitivity and a slight but reproducible increase in CPT sensitivity compared to the *rad55*Δ
407 single mutant (Fig. 4E). Taken together, these results suggested that Rtt107 was not required for
408 the function of Rad55 in the context of resistance to chronic DNA damage.

409 The observations outlined above suggested that Rtt107 cooperated with Rad55 to limit
410 LOH and mitotic RCOs, and we therefore hypothesized that Rtt107 may limit genome instability
411 through a DDR pathway that is known to be regulated by Rad55. Given that Rtt07 may not be
412 required for Rad55's canonical DSB repair function [20], we considered that Rtt107 may
413 cooperate with Rad55 in regulating DNA damage tolerance, as mutants deficient in
414 recombination can rely on tolerance to limit spontaneous LOH [59]. To test our hypothesis, we
415 compared the spontaneous LOH phenotype of the *rtt107*Δ mutant with those of a *rev3*Δ mutant
416 deficient in TLS, a *ubc13*Δ mutant deficient in error-free PRR, and a *rad18*Δ mutant deficient in
417 both pathways [60,61]. Consistent with previous work, the *rad18*Δ mutant exhibited a modest
418 (~2-fold) but significant increase in spontaneous LOH [39] (Fig. S3). The *ubc13*Δ mutation did
419 not affect the rate of spontaneous LOH in wild-type or *rtt107*Δ mutant, indicating that Rtt107 did
420 not primarily limit LOH by promoting error-free PRR. In addition, the *rev3*Δ mutation increased
421 the LOH phenotype of the *rtt107*Δ mutant, although this effect was modest (~1.5-fold). The
422 findings outlined above indicated that Rtt107 acted in the same pathway as Rad55 to limit

423 spontaneous LOH and mitotic RCOs, but that Rtt107 did not cooperate with Rad55 in all
424 contexts.

425 **3.4 The *rad55-S404A* mutation largely disrupted the Rtt107–Rad55 interaction**

426 To further delineate the mechanisms underlying the genetic relationship between *RTT107*
427 and *RAD55*, we tested whether the physical interaction between Rtt107 and Rad55 was important
428 for preventing genome instability. We considered that the Rtt107–Rad55 interaction may be
429 mediated by Rad55-S404 phosphorylation, which does not require DNA damage induction [62],
430 as the Rtt107–Rad55 interaction occurs under normal growth conditions [20]. To test this
431 hypothesis, we generated a *rad55-S404A* mutation and established that it did not affect Rad55
432 protein level (Fig. S4). To determine whether the *rad55-S404A* mutation affected the Rtt107–
433 Rad55 interaction, we performed a small-scale interaction assay using FLAG-Rad55 from log-
434 phase cultures (Fig. 5A). We observed copurification of Rad57-HA and Rtt107-VSV with
435 Rad55, which was consistent with a previous report [20]. The *rad57*Δ mutation did not eliminate
436 the copurification of Rtt107 with Rad55, indicating that the Rtt107–Rad55 interaction was
437 independent of Rad57. As Rtt107 was also found in Rad57 immunoprecipitations [20], these
438 results were consistent with a model in which Rtt107 interacts with Rad55 to form an Rtt107–
439 Rad55–Rad57 trimeric complex. Of note, the *rad55-S404A* mutation substantially reduced the
440 amount of Rtt107, but not Rad57, that copurified with Rad55, suggesting that the Rad55-S404
441 residue was indeed important for the interaction with Rtt107, while having no appreciable effect
442 on the Rad55–Rad57 interaction. For our purposes, we therefore concluded that this mutation
443 was appropriate for investigating the importance of the Rtt107–Rad55 interaction in functional
444 assays.

445 A previous report suggested that mutation of the Rad55-S404 site does not affect the
446 ability of cells to grow during chronic treatment with MMS [62]. As the phenotypes of DNA
447 repair mutants can be highly dependent on the type of DNA-damaging agent used as well as the
448 strain background, we examined whether the *rad55-S404A* mutation affected the ability of our
449 strains to grow during chronic exposure to MMS, HU, or CPT (Fig. 5B). We found that the
450 *rad55-S404A* mutation did not cause sensitivity to any of these agents at concentrations that
451 severely inhibited growth of the *rad55*Δ mutant. Taken together, these observations suggested
452 that the *rad55-S404A* mutation left Rad55 function in this context largely intact and that the
453 interaction between Rtt107 and Rad55 was not crucial for growth during chronic exposure to
454 DNA-damaging agents.

455 **3.5 The *rad55-S404A* mutation increased spontaneous LOH and RCO rates**

456 As the *rad55-S404A* mutation largely disrupted the physical Rtt107–Rad55 interaction,
457 we next used it to examine whether the interaction between Rtt107 and Rad55 contributed to
458 limiting spontaneous genome instability. First, we again employed the bimater assay to examine
459 LOH induced by a broad range of events. The *rad55-S404A* mutation caused a modest (~2-fold)
460 increase in spontaneous LOH in comparison to the wild-type strain (Fig. 6A), consistent with a
461 model in which Rtt107 and Rad55 prevented spontaneous RCOs in part by binding to each other.
462 However, we noted that the *rad55*Δ mutation caused a much greater increase in LOH rate in the
463 bimater assay (~10-fold) (Fig. 4A). Further, the LOH phenotype of the *rtt107*Δ mutant was also
464 greater than that of the *rad55-S404A* point mutant, and the *rtt107*Δ *rad55-S404A* double mutant
465 exhibited a higher rate of LOH than either single mutant alone, suggesting that the function of
466 Rtt107 in preventing LOH may not be solely dependent on the Rad55-S404 site and the Rtt107–
467 Rad55 interaction

468

469 To more granularly determine the types of spontaneous genome instability that may be
470 prevented by Rtt107–Rad55 interaction, we again used the sectoring assay to specifically
471 examine mitotic RCO events. The *rad55-S404A* mutation increased the frequency of mitotic
472 RCOs, indicating that the Rad55-S404 site contributed to the limitation of spontaneous RCOs,
473 and suggesting that the interaction between Rtt107 and Rad55 may be important in this context
474 (Fig. 6B). The *rtt107*Δ *rad55-S404A* double mutant phenotype was similar to that of the *rtt107*Δ
475 single mutant, and this pattern was broadly similar to the epistasis observed between the *rtt107*Δ
476 and *rad55*Δ mutations in the context of the RCO phenotype (Fig. 4B), consistent with a shared
477 role for Rtt107 and the Rad55-S404 site in limiting mitotic RCOs.

478

479 To further delineate the functional relevance of the Rtt107–Rad55 interaction, we
480 considered that the spontaneous LOH and RCO phenotypes of the *rad55-S404A* mutant may be
481 indicative of a defect in a specific DNA repair pathway, possibly the crossover-generating
482 homologous recombination pathway. We therefore examined whether the *rad55-S404A* and
483 *rtt107*Δ mutants exhibited various types of spontaneous genome instability related to
484 recombinational repair using an established assay that discriminates between several distinct
485 types of recombination and mutation in diploid cells (Figure 1) (see [49] for details). In this
486 assay, Class 1/2 events primarily represent RCOs and break-induced replication (BIR) events.
487 Class 3/4 events primarily represent local gene conversions that occur without crossovers, or *de*
488 *novo* mutations occurring within the markers. Class 5/6 events primarily represent loss of one
489 copy of chromosome V by nondisjunction. Using this approach, we found that the *rtt107*Δ
490 mutant exhibited higher rates of Class 1 and Class 3/4 events but wild-type rates of Class 5/6

491 events (Fig. 6C). In the case of Class 2 events, the *rtt107*Δ mutant showed a trend toward a
492 higher spontaneous mutation rate than wild-type, but this increase was not statistically
493 significant. We further examined the Class 3 events in the *rtt107*Δ mutant by colony PCR and
494 found that 24 of 28 events (86%) represented gene conversion rather than *de novo* mutation
495 within the marker (see *Materials and Methods*). These observations suggested that *rtt107*Δ
496 mutants have elevated rates of gene conversion, RCOs, and possibly BIR, but not chromosome
497 loss. The *rad55-S404A* single mutant did not exhibit significantly increased rates in any of these
498 classes, and the *rtt107*Δ *rad55-S404A* double mutant resembled the *rtt107*Δ single mutant. In
499 contrast to the importance of the Rad55-S404 phosphorylation site for limiting LOH and RCOs,
500 these results indicated that Rad55-S404 was not essential to limit multiple other types of
501 spontaneous genome instability that are common in *rtt107*Δ mutants.

502 **3.6 *RTT107* and *RAD55/RAD57* acted in similar genetic pathways under normal growth**
503 **conditions**

504 Our findings suggested that Rtt107 cooperated with Rad55 to limit spontaneous LOH and
505 RCOs, and that this function was at least partially distinct from its role in the response to chronic
506 DNA-damaging agent exposure. Therefore, we hypothesized that the genetic interaction
507 spectrum of *RTT107* drawn from studies that did not apply DNA-damaging agents may provide
508 relevant insights regarding the relations between *RTT107* and *RAD55*, and potentially also
509 *RAD57*. To test this hypothesis, we compared published genetic interaction data on *RTT107*,
510 *RAD55*, and *RAD57* from several high-throughput screens performed under normal growth
511 conditions, and determined which genetic interactions were shared between at least two of these
512 genes (Table 1) [63–71]. Of the 99 genetic interactions shared between *RAD55* and *RAD57*, we
513 found that 40 were also shared with *RTT107.* This represented significant overlap between genes

514 that interacted with *RTT107* and genes that interacted with *RAD55* + *RAD57* (Fisher's exact test,
515 two sided, $p < 2.2 \times 10^{-16}$). Fewer interactions (8) were shared between either *RTT107* + *RAD55*
516 or *RTT107* + *RAD57* only. While further analyses will be required to fully establish the
517 relationships between *RTT107*, *RAD55*, and *RAD57*, the greater than expected by chance overlap
518 of shared genetic interactors suggested that these genes may act, at least in part, in the same
519 pathways under normal growth conditions.

520 **Table 1. Shared and distinct genetic interaction profiles between *RTT107*, *RAD55,* and**

521 ***RAD57***

Shared genetic interaction partners	Genes with shared interactions		Total shared interactions
	Negative interactions	Positive interactions	
RAD55* + *RAD57 (only)	*BCS1*, *BIM1*, *BRE1*, *CIK1*, *CSM3*, *DBF2*, *DEP1*, *DFR1*, *GET1*, *HOM6*, *HSL1*, *HYR1*, *IMG2*, *IRC19*, *LGE1*, *LRS4*, *LSM6*, *LSM7*, *MCM1*, *MDM12*, *MET7*, *MMS22*, *MRC1*, *NAT1*, *NPT1*, *NUP133*, *POL3*, *POL31*, *POL32*, *PRI1*, *PRI2*, *RAD5*, *REV1*, *REV3*, *REV7*, *RFA2*, *RFC2*, *RFC4*, *RFC5*, *RIM1*, *RPN11*, *RPN4*, *RVS161*, *SKN7*, *SOH1*, *SWS2*, *UBP8*, *VAC7*, *VMA3*, *VPS34*, *YAP1*, *YBP1*, *YFH1*, *YJR124C*	*MMS21*, *RAD51*, *RAD52*, *RAD54*, *TOP3*	**59**
RAD55* + *RAD57* + *RTT107	*AIM10*, *ASA1*, *ASF1*, *CCS1*, *CDH1*, *CLA4*, *CSM1*, *CTF18*, *CTF4*, *CTF8*, *DCC1*, *DIA2*, *DOC1*, *DST1*, *DUN1*, *EAF1*, *ELG1*, *GET2*, *LTE1*, *MMS1*, *MON2*, *NPL3*, *NUP60*, *NUP84*, *POL12*, *POL30*, *RAD18*, *RAD27*, *RAD6*, *RFA3*, *RFC1*, *RPN10*, *RPN8*, *RPT1*, *RRM3*, *SLX5*, *SLX8*, *SOD1*, *STP22*, *TSA1*		**40**
RTT107* + *RAD55 (only)	*CCR4*, *CDC9*, *HUR1*, *PMR1*, *POP2*, *RML2*, *SMC5*, *SWI6*		**8**
RTT107* + *RAD57 (only)	*CLB2*, *DOA1*, *ISU1*, *RPN12*, *RPT4*, *SAC3*, *VID22*	*PAT1*	**8**

522

523 The listed genes shared the same type of genetic interaction between at least two of *RTT107*,
524 *RAD55*, and *RAD57*. Gene deletions or loss-of-function alleles of essential genes were used in
525 these studies. "Negative" interactions caused either slower growth or lethality. Note that genes in
526 the "*RAD55* + *RAD57*" row did not also share an interaction with *RTT107*.

527 **4 Discussion**

528 Although Rtt107 is known as a multi-BRCT scaffold with homologs in fission yeast and
529 vertebrates [11], its specific yet important function in limiting spontaneous genome instability
530 phenotypes has remained unclear. Here, we showed that the role of Rtt107 in preventing
531 spontaneous LOH was distinct from its well-characterized functions as a scaffold that localizes
532 to γH2A after induction of DNA damage. Instead, Rtt107 cooperated with the recombination
533 mediator Rad55, at least in part, to limit spontaneous LOH and mitotic RCOs in diploid cells.
534 The Rad55-S404 phosphorylation site was partially required for the Rtt107–Rad55 protein–
535 protein interaction and to limit spontaneous LOH and RCOs, suggesting that the physical
536 interaction between Rtt107 and Rad55 contributed to the suppression of these events. In contrast,
537 the cooperation between Rtt107 and Rad55 did not extend to prevention of all types of
538 spontaneous genome instability. For example, Rtt107 acted in the same pathway as Slx4 to limit
539 rDNA recombination. Taken together, our results indicated that Rtt107 acted with either the
540 recombination mediator Rad55 or its well-characterized binding partner Slx4 to limit types of
541 genome instability that occur spontaneously under normal growth conditions.
542

543 **4.1 Rtt107 limited spontaneous genome instability in distinct pathways**

544 The role of Rtt107 in limiting genome instability differed between various types of
545 instability. Rtt107 cooperated with Rad55 to prevent LOH at the mating locus and mitotic RCOs
546 on chromosome V in diploid cells, likely in part by binding to Rad55 in a manner dependent on
547 Rad55-S404 (Fig. 7A). Our data were also consistent with a model in which Rtt107 interacts
548 with the complete Rad55–Rad57 heterodimer by binding primarily to Rad55, and genetic
549 interaction data suggested that *RTT107*, *RAD55*, and *RAD57* can act in similar pathways under

550 normal growth conditions (Table 1). However, the Rad55-S404 site, while important for
551 mediating the physical interaction between Rad55 and Rtt107, was not needed to limit other
552 types of instability that are common in diploid cells, specifically gene conversion and possibly
553 BIR (Fig. 6C). These observations suggested that Rtt107 primarily acted independently of the
554 Rtt107–Rad55 interaction to limit these events, whereas the Rtt107–Rad55 interaction may
555 specifically limit LOH and mitotic RCOs. We also found that the function of Rtt107 in the
556 context of LOH was dependent on BRCT5/6 but independent of the Rtt107-K887 residue that
557 mediates interaction with γH2A (Fig. 2B) [10,19]. This was in contrast to earlier observations
558 indicating that *rtt107-K887M* and *rtt107ΔBRCT5/6* mutants exhibit similar phenotypes with
559 respect to growth during chronic MMS treatment and the recruitment of Rtt107 to induced DSBs
560 [10]. Interestingly, the structure of BRCT5/6 is remarkably flexible, and protein binding via
561 BRCT5/6 using surfaces other than the γH2A-binding pocket has been proposed previously [19].
562 Taken together, these findings suggested that Rtt107–BRCT5/6 may bind to a non-γH2A partner
563 and thus prevent LOH (Fig. 7A), and the identification of such a partner represents an
564 opportunity for future research. It is of interest to consider that Rad55 binds to Rtt107–BRCT1–4
565 [14,20], and that Rtt107 may act to bridge Rad55, or the complete Rad55–Rad57 heterodimer, to
566 a partner that binds BRCT5/6.

567 Rtt107 cooperated with Slx4 to prevent hyperrecombination at the rDNA locus in haploid
568 cells, while not depending primarily on Rad55 in this context. Recent work suggested that Rtt107
569 limits rDNA recombination at least in part as a γH2A-binding scaffold for its physical interaction
570 partners, including Slx4 [14]. Therefore, the cooperation of Rtt107 with Slx4 in rDNA
571 maintenance may involve binding to γH2A via Rtt107–BRCT5/6 (Fig. 7B). We note that Rtt107

572 did not rely on Slx4 to prevent spontaneous LOH (Fig. 3A), again suggesting that Rtt107 acts in
573 different pathways to limit different types of spontaneous genome instability.
574 In addition to the spontaneous genome instability phenotypes examined in this study, the
575 *rtt107*Δ mutant exhibits elevated levels of spontaneous DNA damage foci in S/G_2/M phase
576 [15,25,38]. Interestingly, the *rtt107*Δ mutation does not exhibit broad epistasis with mutations of
577 canonical DNA damage repair or tolerance pathways [8,20,44,72,73]. Taken together, these
578 findings were consistent with a model in which Rtt107 maintains genome stability at least in part
579 by limiting the levels of DNA damage that occur during replication, rather than by directly
580 affecting a specific repair process or pathway choice. Furthermore, it is interesting that DSBs
581 appear to be the primary initiator of spontaneous crossovers in yeast [74–76]. The dispensability
582 of Rtt107 for survival after exposure to DSB-inducing ionizing radiation [8], along with the
583 requirement for Rtt107 in preventing spontaneous crossovers, could be reconciled by a model in
584 which Rtt107 prevents the occurrence of DSBs but is not essential for DSB repair.
585

586 **4.2 Cooperation between Rtt107 and Rad55 in genome maintenance**

587 Our genetic evidence suggested that Rtt107 interacted with Rad55 to limit rates of
588 spontaneous RCOs, and functioned at least in part with Rad55 to limit LOH. We note that the
589 LOH phenotype examined in this study could have been largely driven by mitotic RCO events,
590 and that these phenotypes would be consistent with a relationship between the Rtt107–Rad55
591 interaction and recombinational repair pathways, which are mediated by Rad55–Rad57.
592 However, it remains unclear how Rtt107 and Rad55 would cooperate to prevent spontaneous
593 genome instability. In complexes such as Rtt107–Slx4, Rtt107–SMC5/6, or Rtt107–Rtt101–
594 Mms1–Mms22, Rtt107 has commonly been proposed to act as a scaffold that recruits its binding

595 partners to γH2A near DNA damage lesions (Fig. 7B) [9,10,14,16,55]. In contrast, our results
596 presented here suggested that Rtt107–γH2A binding was actually dispensable for the function of
597 Rtt107 in preventing LOH, and a model in which Rtt107 simply recruits Rad55 to lesions thus
598 appears less applicable. Rtt107 and Rad55 also localize to different DNA damage signals, as
599 Rad55 associates with the Rad51–ssDNA filament during recombination [26,77], while Rad51
600 does not appear to assemble nonspecifically onto double-stranded DNA [78]. Rtt107 localizes to
601 the histone marks γH2A and H4T80ph, which flank DSB sites and are excluded from ssDNA
602 [7,10,78]. Therefore, while Rtt107 and Rad55 both localize near DSBs in broad terms, their
603 known recruitment pathways appear to target different regions around DSBs. Rad51 can be
604 detected in similar regions to γH2A due to homology search performed by the Rad51 filament
605 [78], but it is unclear whether the Rtt107–Rad55 interaction is important during homology search
606 or some other process. Alternatively, Rtt107 and Rad55 may cooperate at sites other than DSBs,
607 such as stalled replication forks. The localization of Rtt107 behind stressed replication forks has
608 been shown to be γH2A-dependent [13], whereas the recruitment of Rad55 to replication forks is
609 less well understood [79,80] and it is unclear whether Rtt107 and Rad55 can be recruited to
610 stressed forks at similar times.
611
612 While our findings were consistent with a relationship between the Rtt107–Rad55
613 interaction and recombinational repair, it is also important to note that Rtt107 does not suppress
614 recombination at all loci. For example, a genome-wide study that identified rDNA
615 hyperrecombination in the *rtt107*Δ mutant found normal rates of recombination at the *LEU2*
616 locus in two assays [38].

617 We found that the Rad55-S404 phosphorylation site was important for the physical
618 interaction between Rtt107–Rad55 and for limiting mitotic RCOs and LOH. However, in the
619 context of the LOH phenotype, we did not identify clear epistasis between the *rtt107*Δ and
620 *rad55-S404A* mutations (Fig. 6A), which suggested that the Rad55-S404 site may have roles in
621 Rad55's function beyond the complexes or pathways involving Rtt107. Further, it is possible that
622 residual binding between Rtt107 and Rad55 occurs in the *rad55-S404A* mutant, limiting the
623 impact of the targeted *rad55-S404A* mutation on certain genome instability phenotypes, although
624 this was not detectable in the assays employed here. In contrast, we observed epistasis between
625 the *rtt107*Δ and *rad55*Δ mutations in the context of the LOH phenotype (Fig. 3F and 4A),
626 suggesting that Rtt107 and Rad55 act broadly in the same pathway to prevent LOH.
627 It should also be noted that we identified cooperation between Rtt107 and Rad55 in
628 assays using diploid yeast, whereas Rtt107 did not cooperate primarily with Rad55 to prevent
629 rDNA recombination in haploids (Fig. 4D). Diploid and haploid yeast differ in DDR regulation,
630 with diploids utilizing HR over NHEJ for DSB repair [30]. Further, the sensitivity of *rad55*Δ
631 mutants to ionizing radiation is suppressed by heterozygosity at the mating locus, which occurs
632 naturally in diploids [30,31]. Therefore, the degree of cooperation between Rtt107 and Rad55 in
633 genome maintenance may be partly dependent on ploidy.
634 We identified a spontaneous LOH phenotype for an *rtt107-K426M* mutant (Fig. 2B),
635 suggesting that the K426-dependent interaction of Rtt107 with phosphorylated H4T80 may also
636 be important for preventing spontaneous LOH, possibly by affecting the timing of Rtt107
637 recruitment [7]. However, we note that K426 is within Rtt107–BRCT1–4, and that BRCT1–4
638 interacts with a number of interaction partners of Rtt107, including Rad55 [9,14,15,20].

639 Therefore, it remains possible that the *rtt107-K426M* mutation could also affect the Rtt107–
640 Rad55 complex, or other Rtt107 complexes.
641

642 **4.3 Cooperation between Rtt107 and Slx4 in rDNA maintenance**

643 We found that Rtt107 acted in the same pathway as Slx4 to maintain rDNA stability (Fig.
644 S2). The role of Rtt107 in rDNA maintenance may be similar to its role in GCR suppression in
645 haploid cells, in which Rtt107 acts at least in part as a γH2A-binding scaffold for Slx4, Mms22,
646 and Nse6 (Fig. 7B) [9,14,15,20]. It is not yet clear whether Rtt107 also cooperates with the Slx1
647 endonuclease in this context. Although an Rtt107–Slx1–Slx4 complex has been identified [15],
648 Rtt107 has not been previously implicated in the endonuclease function of Slx1–Slx4. In
649 addition, we note that the rDNA hyperrecombination phenotype of the *slx4*Δ mutant identified in
650 this study differs from a previous report in which the *slx4*Δ mutant exhibited lower rates of
651 rDNA recombination than wild-type [81]. This discrepancy may be related to measurement of
652 the loss of a single *ADE2* marker in the rDNA in the earlier study, rather than the combined
653 *ADE2-CAN1* marker used here and in a recent study identifying rDNA hyperrecombination in an
654 *slx4* mutant [14,50]. Relatedly, the *Schizosaccharomyces pombe* homolog of Rtt107, Brc1, has
655 been proposed to play a role in genome maintenance in regions that are susceptible to replication
656 stress, including the rDNA [82], likely at least in part due to recruitment of Brc1 to γH2A, with
657 the γH2A–Brc1 foci colocalizing with rDNA [83].

658 Recent work identified GCR and rDNA recombination phenotypes for mutations of the
659 Rtt107 interaction motifs (RIMs) that are important for the interaction between Rtt107–BRCT1–
660 4 and three of the binding partners of Rtt107, i.e., Slx4, Mms22, and the SMC5/6 subunit, Nse6
661 [14]. These *RIM* mutants each exhibited mild rDNA hyperrecombination phenotypes in

662 comparison to the more pronounced phenotype of the *rtt107*Δ mutant, suggesting that individual
663 interactions may have had limited or partially redundant contributions to the rDNA maintenance
664 function of Rtt107. Our results were consistent with substantial cooperation between Rtt107 and
665 Slx4 in rDNA maintenance, as the *slx4*Δ and *rtt107*Δ mutations had similar and epistatic effects
666 on rDNA stability (Fig. S2).
667

668 **4.4 Distinct roles for Rtt107 in genome maintenance and DNA damage resistance**

669 In this study, we found that the *rad9-2A* and *H2A-S129A* mutations increased the LOH
670 rate of the *rtt107*Δ mutant (Fig. S1 and 2C), despite suppressing the hypersensitivity of the
671 *rtt107*Δ mutant to chronic MMS treatment [16,17,22]. Previously, we reported a similar pattern
672 in which the *dot1*Δ mutation suppressed the MMS sensitivity of the *rtt107*Δ mutant, but did not
673 suppress its spontaneous LOH phenotype [25]. Each of these mutations that suppress the MMS
674 sensitivity of the *rtt107*Δ mutant can also dampen DNA damage checkpoint activity [53,84–87],
675 and the *H2A-S129A* mutation additionally suppresses the MMS-induced checkpoint
676 hyperactivation phenotype of the *rtt107*Δ mutant [16,17]. The lack of suppression by these
677 mutations of the LOH phenotype in the *rtt107*Δ mutant reported here suggested that the role of
678 Rtt107 in preventing spontaneous LOH was largely distinct from its role in preventing treatment-
679 induced checkpoint hyperactivation. This distinction was further emphasized by the observations
680 that the *rtt107*Δ and *rad55*Δ mutations exhibited epistasis in the context of the LOH phenotype
681 (Fig. 3F and 4A) and a negative genetic interaction in the context of growth during MMS
682 exposure (Fig. 4E) [20]. We also found that *rtt107*Δ mutation suppressed the LOH phenotype of
683 the *mms22*Δ mutant (Fig. 3C), despite the additive effects of *rtt107*Δ and *rtt101*Δ mutations on
684 MMS sensitivity observed in a growth assay [88]. Taken together, these findings indicated that

685 while abundant information is available on the genetic interactions of the *rtt107*Δ mutant in the
686 context of exposure to DNA-damaging agents, these data may not directly reflect the function of
687 Rtt107 in preventing spontaneous LOH.
688
689 The lack of a DNA damage sensitivity phenotype for the *rad55-S404A* mutant suggested
690 that the Rtt107–Rad55 interaction was not important for DNA damage resistance (Fig. 5B). This
691 was unsurprising, as the *rtt107*Δ mutant was less sensitive to DNA-damaging agents than the
692 *rad55*Δ mutant (Fig. 4E). In addition, a previous genome-wide screen in a different genetic
693 background performed in our laboratory revealed a negative genetic interaction between the
694 *rtt107*Δ and *rad55*Δ mutations in the context of CPT sensitivity [73]. However, there was no
695 clear negative interaction between the *rtt107*Δ and *rad55*Δ mutations at this CPT concentration
696 in the W303 *RAD5* genetic background, although the sensitivity of the *rtt107*Δ *rad55*Δ double
697 mutant was slightly greater than that of the *rad55*Δ single mutant (Fig. 4E).
698
699 Taken together, the findings presented here showed that Rtt107 plays multiple roles in the
700 prevention of spontaneous genome instability, which are often distinct from its previously
701 studied functions in the response to DNA-damaging treatments. Further studies are required to
702 determine the specific mechanisms by which Rtt107 prevents various types of genome instability
703 with its diverse interaction partners, including Rad55 and Slx4.

Acknowledgments

We thank G. Leung for preliminary work in strain construction; W. D. Heyer, J. Diffley, C. D. Allis, B. Pfander, L. Aragon, and J. Krebs for generously providing yeast strains and plasmids; and M. Aristizabal, P. Stirling, W. D. Heyer, and A. Kerr for critical reading of the manuscript and suggestions.

709 **Figure Captions**

710 **Fig. 1. Targeted spontaneous genome instability assays used in this study.**

711 The locations of mutations and genomic rearrangements in each assay are shown. All assays
712 were performed under normal growth conditions. The graph colors shown on the right
713 correspond to the colors of graphs for each assay in subsequent figures.

714 **Fig. 2. Rtt107–BRCT1–4 and Rtt107–BRCT5/6 were important for limiting spontaneous**
715 **LOH.**

716 A) Rtt107 structural features mutated in panel B. BRCT domains are numbered and
717 shown in gray. Target lysines are labeled in the center of the BRCT domain in which they are
718 located. The orange circle indicates the SQ/TQ cluster of Rtt107, targeted by the *rtt107-4A*
719 mutation. B) Rtt107-K426 and Rtt107–BRCT5/6 contributed to genome maintenance in the
720 bimater assay, performed using homozygous diploid strains. Mating rates and 95% confidence
721 intervals were calculated using the maximum likelihood method, and statistical significance was
722 assessed by the non-overlap of confidence intervals (see *Materials and Methods*). +, non-overlap
723 of 95% confidence intervals between two strains (statistically significant); ns, overlap of
724 confidence intervals (not significant). Strains indicated in this panel were in the W303 *RAD5*
725 background, and were grown in SC-Leu. At least eight independent colonies were tested. C)
726 Rtt107 prevented spontaneous LOH independently of γH2A in the bimater assay. The *H2A-*
727 *S129A* mutation caused genome instability, and the *rtt107*Δ *H2A-S129A* double mutant
728 phenotype was greater than those of either single mutant. Mating rates and 95% confidence
729 intervals were calculated and compared as described for panel B. Eleven independent colonies
730 were tested.

731 **Fig. 3. Rtt107 limited spontaneous LOH in the same pathway as Rad55.**

732 All panels depict bimater assays. The mating rates and 95% confidence intervals were calculated
733 and compared as described for the bimater assay in Figure 2B. ns, overlap of confidence
734 intervals (not significant). A simplified model of the corresponding physical interaction of
735 Rtt107 is indicated beneath each assay, and mutated complex members are shown in color.
736 Experiments were performed in the W303 *rad5-535* background except where noted. Note that
737 the scale on the *y*-axis differs between panels.
738 A) The *slx4*Δ mutation did not increase the rate of spontaneous LOH or affect the *rtt107*Δ mutant
739 phenotype. At least six independent colonies were tested. B) The *smc6-9* mutation caused far
740 greater instability in the bimater assay than the *rtt107*Δ mutant. The phenotype of the *rtt107*Δ
741 *smc6-9* double mutant was not distinguishable from that of the *smc6-9* single mutant. At least
742 seven independent colonies were tested. C) The *mms22*Δ mutation caused instability in the
743 bimater assay. The *mms22*Δ mutant exhibited a higher rate of LOH than the *rtt107*Δ mutant, and
744 this phenotype was suppressed by the *rtt107*Δ mutation. Ten to thirteen independent colonies
745 were tested. D) The *rtt107*Δ *mms4-8A* double mutant exhibited a greater rate of LOH than either
746 single mutant in the bimater assay. At least seven independent colonies were tested. Note that
747 this experiment was performed in the W303 *RAD5* background, and that the complex model
748 depicted in this panel is a hypothetical arrangement. E) The *sgs1*Δ mutant exhibited a higher
749 LOH rate than the *rtt107*Δ mutant in the bimater assay. The *rtt107*Δ *sgs1*Δ double mutant
750 exhibited a higher LOH rate than either single mutant. Eleven independent colonies were tested.
751 F) The *rtt107*Δ *rad55*Δ double mutant exhibited a similar LOH rate to the *rtt107*Δ and *rad55*Δ
752 single mutants. At least 12 independent colonies were tested.
753 **Fig. 4. Rtt107 and Rad55 limited spontaneous mitotic RCO frequency in the same pathway.**

754 Experiments were performed in the W303 *RAD5* background. Rates and 95% confidence
755 intervals for the bimater assay (panel A), ALF assay (panel C), and rDNA instability assay
756 (panel D) were calculated and compared as described for the bimater assay in Figure 2B. +, non-
757 overlap of 95% confidence intervals between two strains (statistically significant); ns, overlap of
758 confidence intervals (not significant). A) The *rtt107*Δ *rad55*Δ double mutant exhibited a similar
759 LOH rate to the *rad55*Δ single mutant in the bimater assay. Findings were similar to those in the
760 W303 *rad5-535* background (Fig. 3F). Eight to 10 independent colonies were tested. B) The
761 *rtt107*Δ, *rad55*Δ, and *rtt107*Δ *rad55*Δ mutants exhibited a similar increase in spontaneous mitotic
762 RCO frequency. Canavanine-resistant sectored colonies were scored as representative of RCOs.
763 Frequencies were calculated from 13–16 independent colonies. **, $p < 0.01$, *** $p < 0.005$
764 compared to the wild-type (Student's *t* test). C) The *rtt107*Δ and *rad55*Δ mutants exhibited a
765 higher rate of instability in the haploid ALF assay. The phenotype of the *rtt107*Δ *rad55*Δ double
766 mutant showed a trend toward a higher rate than the *rtt107*Δ mutant, but this difference was not
767 statistically significant. Haploid strains were used to determine mating rates in the ALF assay,
768 and 7–9 independent colonies were tested. D) The *rtt107*Δ and *rad55*Δ mutants exhibited a
769 higher rate of spontaneous rDNA recombination in comparison to wild-type. The *rtt107*Δ mutant
770 and *rtt107*Δ *rad55*Δ double mutant showed a higher rate of rDNA recombination than the
771 *rad55*Δ mutant. rDNA recombination was measured as the loss of an *ADE2-CAN1* marker in the
772 rDNA, and eight independent colonies were tested. E) The *rtt107*Δ *rad55*Δ double mutant
773 showed greater sensitivity to MMS treatment than either single mutant. Tenfold serial dilutions
774 from overnight cultures were plated on media containing the indicated concentrations of DNA-
775 damaging agents, and then incubated for 2 days at 30°C.

776 **Fig. 5. A *rad55-S404A* mutation largely disrupted the physical Rtt107–Rad55 interaction,**
777 **but did not clearly affect growth during chronic exposure to DNA-damaging agents.**

778 Experiments were performed in the W303 *RAD5* background. A) The *rad55-S404A* mutation
779 greatly reduced the amount of Rtt107 that co-purified with Rad55, but left Rad55–Rad57
780 interaction largely intact. Co-purification of Rtt107 with Rad55 did not require *RAD57.* FLAG
781 purification was performed on log-phase cultures. Immunoblotting was performed using anti-
782 FLAG, anti-VSV, and anti-HA antibodies. Anti-PGK1 antibody was applied to the input fraction
783 as a loading control, due to the poor visibility of FLAG-Rad55 and Rad57-HA in whole cell
784 extract. B) The *rad55-S404A* mutation or N-terminal 3×FLAG tag on Rad55 did not affect DNA
785 damage sensitivity. Higher concentrations of DNA-damaging agents were used to examine the
786 sensitivity of the *rad55-S404A* mutant, and the *rad55*Δ mutant was included for comparison.
787 Tenfold serial dilutions of overnight cultures were plated on media containing the indicated
788 concentrations of DNA-damaging agents, and then incubated for 2 days at 30°C.

789 **Fig. 6. The *rad55-S404A* mutation increased spontaneous rates of LOH and mitotic RCOs.**
790 Experiments were performed in the W303 *RAD5* background. A) The *rad55-S404A* mutation
791 caused a higher rate of LOH in the bimater assay, but did not exhibit epistasis with the *rtt107*Δ
792 mutation. Mating rates were calculated from 10–12 independent colonies as described for the
793 bimater assay in Figure 2B. +, non-overlap of 95% confidence intervals between two strains
794 (statistically significant); ns, overlap of confidence intervals (not significant). B) The *rad55-*
795 *S404A* mutation increased the frequency of mitotic RCOs, and the *rad55-S404A rtt107*Δ double
796 mutant phenotype was similar to that of the *rtt107*Δ mutant. Frequencies were calculated from
797 20–21 independent colonies. *, $p < 0.05$; **, $p < 0.01$, ***, $p < 0.005$ compared to the wild-type
798 (Student's *t* test). C) The *rtt107*Δ mutant exhibited multiple types of spontaneous genome
799 instability, and these phenotypes were not significantly affected by the *rad55-S404A* mutation.
800 Six phenotypic classes of colony were scored using an assay for several types of mutation and

801 mitotic recombination events. Rates were calculated and compared as described for the bimater
802 assay in Figure 2B. +, non-overlap of 95% confidence intervals between two strains (statistically
803 significant); ns, overlap of confidence intervals (not significant). Eight to nine independent
804 colonies were tested for Class 1–4 events, and five to six colonies were tested for Class 5/6
805 events.

806 **Fig. 7. Rtt107 acts with different partners to prevent various types of genome instability.**
807 The dotted lines indicate physical interactions between Rtt107 and proteins that maintain
808 stability in the same pathway. Numbered gray boxes indicate Rtt107 BRCT domains. A) Rtt107
809 prevents spontaneous LOH and mitotic RCOs by cooperating with the Rad55–Rad57
810 heterodimer, which binds to Rtt107–BRCT1–4. The Rad55-S404 phosphorylation site
811 contributes to the Rtt107–Rad55 interaction. Rtt107–BRCT5/6 contributes to the function of
812 Rtt107 in preventing LOH events, possibly by binding to a partner other than γH2A. B) Rtt107
813 prevents rDNA recombination by cooperating with Slx4, which binds to Rtt107–BRCT1–4.
814 Rtt107 may act as a γH2A-binding scaffold that recruits Slx4 near lesions in this context.

815 **References**

816 1. Ciccia A, Elledge SJ. The DNA damage response: making it safe to play with knives. Mol
817 Cell. 2011;40: 179–204. doi:10.1016/j.molcel.2010.09.019

818 2. Putnam CD, Kolodner RD. Pathways and mechanisms that prevent genome instability in
819 Saccharomyces cerevisiae. Genetics. 2017;206: 1187–1225.
820 doi:10.1534/genetics.112.145805

821 3. Mehta A, Haber JE. Sources of DNA double-strand breaks and models of recombinational
822 DNA repair. Cold Spring Harb Perspect Biol. 2014;6: 016428–016428.
823 doi:10.1101/cshperspect.a016428

824 4. Emerson CH, Bertuch AA. Consider the workhorse: Nonhomologous end-joining in
825 budding yeast. Biochemistry and Cell Biology. 2016;94: 396–406. doi:10.1139/bcb-2016-
826 0001

827 5. Pizzul P, Casari E, Gnugnoli M, Rinaldi C, Corallo F, Longhese MP. The DNA damage
828 checkpoint: A tale from budding yeast. Front Genet. 2022;13: 995163.
829 doi:10.3389/fgene.2022.995163

830 6. van Attikum H, Gasser SM. The histone code at DNA breaks: a guide to repair? Nature
831 reviews Molecular cell biology. 2005;6: 757–65. doi:10.1038/nrm1737

832 7. Millan-Zambrano G, Santos-Rosa H, Puddu F, Robson SC, Jackson SP, Kouzarides T.
833 Phosphorylation of histone H4T80 triggers DNA damage checkpoint recovery. Mol Cell.
834 2018;72: 625-635 4. doi:10.1016/j.molcel.2018.09.023

835 8. Rouse J. Esc4p, a new target of Mec1p (ATR), promotes resumption of DNA synthesis
836 after DNA damage. The EMBO journal. 2004;23: 1188–97. doi:10.1038/sj.emboj.7600129

837 9. Leung GP, Lee L, Schmidt TI, Shirahige K, Kobor MS. Rtt107 is required for recruitment
838 of the SMC5/6 complex to DNA double strand breaks. Journal of Biological Chemistry.
839 2011;286: 26250–26257. doi:10.1074/jbc.M111.235200

840 10. Leung GP, Brown JAR, Glover JNM, Kobor MS. Rtt107 BRCT domains act as a targeting
841 module in the DNA damage response. DNA Repair. 2016;37: 22–32.
842 doi:10.1016/j.dnarep.2015.10.007

843 11. Wan B, Hang LE, Zhao X. Multi-BRCT scaffolds use distinct strategies to support genome
844 maintenance. Cell Cycle. 2016;15: 2561–2570. doi:10.1080/15384101.2016.1218102

845 12. Roberts TM, Zaidi IW, Vaisica JA, Peter M, Brown GW. Regulation of Rtt107 recruitment
846 to stalled DNA replication forks by the Cullin Rtt101 and the Rtt109 acetyltransferase. Mol
847 Biol Cell. 2008;19: 171–180. doi:10.1091/mbc.e07-09-0961

848 13. Balint A, Kim T, Gallo D, Cussiol JR, Bastos de Oliveira FM, Yimit A, et al. Assembly of
849 Slx4 signaling complexes behind DNA replication forks. The EMBO Journal. 2015;34:
850 2182–2197. doi:10.15252/embj.201591190

851 14. Wan B, Wu J, Meng X, Lei M, Zhao X. Molecular basis for control of diverse genome
852 stability factors by the Multi-BRCT scaffold Rtt107. Mol Cell. 2019;75: 238-251 5.
853 doi:10.1016/j.molcel.2019.05.035

854 15. Roberts TM, Kobor MS, Bastin-Shanower SA, Ii M, Horte SA, Gin JW, et al. Slx4
855 Regulates DNA Damage Checkpoint-dependent Phosphorylation of the BRCT Domain
856 Protein Rtt107/Esc4. Molecular Biology of the Cell. 2006;17: 539–548.
857 doi:10.1091/mbc.e05-08-0785

858 16. Ohouo PY, Oliveira FM, Liu Y, Ma CJ, Smolka MB. DNA-repair scaffolds dampen
859 checkpoint signalling by counteracting the adaptor Rad9. Nature. 2013;493: 120–124.
860 doi:10.1038/nature11658

861 17. Brown JAR, Kobor MS. Budding yeast Rtt107 prevents checkpoint hyperactivation after
862 replicative stress by limiting DNA damage. DNA Repair. 2019;74: 1–16.
863 doi:10.1016/j.dnarep.2019.01.001

864 18. Leung CCY, Glover JNM. BRCT domains: easy as one, two, three. Cell Cycle. 2011;10:
865 2461–2470. doi:10.4161/cc.10.15.16312

866 19. Li X, Liu K, Li F, Wang J, Huang H, Wu J, et al. Structure of C-terminal tandem BRCT
867 repeats of Rtt107 protein reveals critical role in interaction with phosphorylated histone
868 H2A during DNA damage repair. The Journal of biological chemistry. 2012;287: 9137–46.
869 doi:10.1074/jbc.M111.311860

870 20. Chin JK, Bashkirov VI, Heyer W-D, Romesberg FE. Esc4/Rtt107 and the control of
871 recombination during replication. DNA Repair. 2006;5: 618–628.
872 doi:10.1016/j.dnarep.2006.02.005

873 21. Ohouo PY, Oliveira FM, Almeida BS, Smolka MB. DNA damage signaling recruits the
874 Rtt107-Slx4 scaffolds via Dpb11 to mediate replication stress response. Mol Cell. 2010;39:
875 300–306. doi:10.1016/j.molcel.2010.06.019.

876 22. Dibitetto D, Ferrari M, Rawal CC, Balint A, Kim T, Zhang Z. Slx4 and Rtt107 control
877 checkpoint signalling and DNA resection at double-strand breaks. Nucleic Acids Res.
878 2016;44: 669–682. doi:10.1093/nar/gkv1080

879 23. Jablonowski CM, Cussiol J, Oberly S, Yimit A, Balint A, Kim T, et al. Termination of
880 replication stress signaling via concerted action of the Slx4 scaffold and the PP4
881 phosphatase. Genetics. 2015;201: 937–949. doi:10.1534/genetics.115.181479

882 24. Cussiol JR, Jablonowski CM, Yimit A, Brown GW, Smolka MB. Dampening DNA damage
883 checkpoint signalling via coordinated BRCT domain interactions. The EMBO journal.
884 2015;34: e201490834. doi:10.15252/embj.201490834

885 25. Lévesque N, Leung GP, Fok AK, Schmidt TI, Kobor MS. Loss of H3 K79 trimethylation
886 leads to suppression of Rtt107-dependent DNA damage sensitivity through the translesion
887 synthesis pathway. The Journal of biological chemistry. 2010;285: 35113–22.
888 doi:10.1074/jbc.M110.116855

889 26. Sung P. Yeast Rad55 and Rad57 proteins form a heterodimer that functions with replication
890 protein A to promote DNA strand exchange by Rad51 recombinase. Genes and
891 Development. 1997;11: 1111–1121. doi:10.1101/gad.11.9.1111

892 27. Liu J, Renault L, Veaute X, Fabre F, Stahlberg H, Heyer W-D. Rad51 paralogues Rad55-
893 Rad57 balance the antirecombinase Srs2 in Rad51 filament formation. Nature. 2011;479:
894 245–248. doi:10.1038/nature10522

895 28. Sugawara N, Wang X, Haber JE. In vivo roles of Rad52, Rad54, and Rad55 proteins in
896 Rad51-mediated recombination. Mol Cell. 2003;12: 209–219. doi:10.1016/s1097-
897 2765(03)00269-7

898 29. Roy U, Kwon Y, Marie L, Symington L, Sung P, Lisby M. Rad51 paralog complex Rad55-
899 Rad57 acts as a molecular chaperone during homologous recombination. Mol Cell.
900 2020;81: 1–15. doi:10.1016/j.molcel.2020.12.019

901 30. Symington LS, Rothstein R, Lisby M. Mechanisms and regulation of mitotic recombination
902 in *Saccharomyces cerevisiae*. Genetics. 2014;198: 795–835.
903 doi:10.1534/genetics.114.166140

904 31. Lovett ST, Mortimer RK. Characterization of null mutants of the RAD55 gene of
905 Saccharomyces cerevisiae: effects of temperature, osmotic strength and mating type.
906 Genetics. 1987;116: 547–553. doi:10.1093/genetics/116.4.547

907 32. Berti M, Vindigni A. Replication stress: Getting back on track. Nature Structural and
908 Molecular Biology. 2016. pp. 103–109. doi:10.1038/nsmb.3163

909 33. Gaines WA, Godin SK, Kabbinavar FF, Rao T, VanDemark AP, Sung P. Promotion of
910 presynaptic filament assembly by the ensemble of S. cerevisiae Rad51 paralogues with
911 Rad52. Nat Commun. 2015;6: 7834. doi:10.1038/ncomms8834

912 34. Ball LG, Zhang K, Cobb JA, Boone C, Xiao W. The yeast Shu complex couples error-free
913 post-replication repair to homologous recombination. Molecular microbiology. 2009;73:
914 89–102. doi:10.1111/j.1365-2958.2009.06748.x

915 35. Vanoli F, Fumasoni M, Szakal B, Maloisel L, Branzei D. Replication and recombination
916 factors contributing to recombination-dependent bypass of DNA lesions by template
917 switch. PLoS Genet. 2010;6: 1001205. doi:10.1371/journal.pgen.1001205

918 36. Bonilla B, Brown AJ, Hengel SR, Rapchak KS, Mitchell D, Pressimone CA, et al. The Shu
919 complex prevents mutagenesis and cytotoxicity of single-strand specific alkylation lesions.
920 Aguilera A, Tyler JK, editors. eLife. 2021;10: e68080. doi:10.7554/eLife.68080

921 37. Maloisel L, Ma E, Phipps J, Deshayes A, Mattarocci S, Marcand S, et al. Rad51 filaments
922 assembled in the absence of the complex formed by the Rad51 paralogs Rad55 and Rad57
923 are outcompeted by translesion DNA polymerases on UV-induced ssDNA gaps. PLoS
924 Genet. 2023;19: e1010639. doi:10.1371/journal.pgen.1010639

925 38. Alvaro D, Lisby M, Rothstein R. Genome-wide analysis of Rad52 foci reveals diverse
926 mechanisms impacting recombination. PLoS Genet. 2007;3: 228.
927 doi:10.1371/journal.pgen.0030228

928 39. Yuen KWY, Warren CD, Chen O, Kwok T, Hieter P, Spencer FA. Systematic genome
929 instability screens in yeast and their potential relevance to cancer. Proceedings of the
930 National Academy of Sciences of the United States of America. 2007;104: 3925–30.
931 doi:10.1073/pnas.0610642104

932 40. Hendry JA, Tan G, Ou J, Boone C, Brown GW. Leveraging DNA damage response
933 signaling to identify yeast genes controlling genome stability. G3 (Bethesda). 2015;5: 997–
934 1006. doi:10.1534/g3.115.016576

935 41. Putnam CD, Hayes TK, Kolodner RD. Specific pathways prevent duplication-mediated
936 genome rearrangements. Nature. 2009;460: 984–989. doi:10.1038/nature08217

937 42. Putnam CD, Allen-Soltero SR, Martinez SL, Chan JE, Hayes TK, Kolodner RD.
938 Bioinformatic identification of genes suppressing genome instability. Proc Natl Acad Sci U
939 S A. 2012;109: E3251-3259. doi:10.1073/pnas.1216733109

940 43. Kobayashi T. Regulation of ribosomal RNA gene copy number and its role in modulating
941 genome integrity and evolutionary adaptability in yeast. Cellular and Molecular Life
942 Sciences. 2011;68: 1395–1403. doi:10.1007/s00018-010-0613-2

943 44. Hang LEE, Peng J, Tan W, Szakal B, Menolfi D, Sheng Z. Rtt107 is a multi-functional
944 scaffold supporting replication progression with partner SUMO and ubiquitin ligases. Mol
945 Cell. 2015;60: 268–279. doi:10.1016/j.molcel.2015.08.023

946 45. Princz LN, Wild P, Bittmann J, Aguado FJ, Blanco MG, Matos J, et al. Dbf4-dependent
947 kinase and the Rtt107 scaffold promote Mus81-Mms4 resolvase activation during mitosis.
948 The EMBO Journal. 2017;36: e201694831. doi:10.15252/embj.201694831

949 46. Ho Y, Gruhler A, Heilbut A, Bader GD, Moore L, Adams SL. Systematic identification of
950 protein complexes in *Saccharomyces cerevisiae* by mass spectrometry. Nature. 2002;415:
951 180–183. doi:10.1038/415180a

952 47. Zheng Q. rSalvador: An R package for the fluctuation experiment. G3: Genes, Genomes,
953 Genetics. 2017;7: 3849–3856. doi:10.1534/g3.117.300120

954 48. Zheng Q. Methods for comparing mutation rates using fluctuation assay data. Mutation
955 Research - Fundamental and Molecular Mechanisms of Mutagenesis. 2015;777: 20–22.
956 doi:10.1016/j.mrfmmm.2015.04.002

957 49. Barbera MA, Petes TD. Selection and analysis of spontaneous reciprocal mitotic cross-
958 overs in Saccharomyces cerevisiae. Proceedings of the National Academy of Sciences of
959 the United States of America. 2006;103: 12819–12824. doi:10.1073/pnas.0605778103

960 50. Fritze CE, Verschueren K, Strich R, Easton Esposito R. Direct evidence for SIR2
961 modulation of chromatin structure in yeast rDNA. EMBO J. 1997;16: 6495–509.
962 doi:10.1093/emboj/16.21.6495

963 51. Kobor MS, Venkatasubrahmanyam S, Meneghini MD, Gin JW, Jennings JL, Link AJ. A
964 protein complex containing the conserved Swi2/Snf2-related ATPase Swr1p deposits
965 histone variant H2A.Z into euchromatin. PLoS Biol. 2004;2: 131.
966 doi:10.1371/journal.pbio.0020131

967 52. Downs JA, Lowndes NF, Jackson SP. A role for *Saccharomyces cerevisiae* histone H2A in
968 DNA repair. Nature. 2000;408: 1001–1004. doi:10.1038/35050000

969 53. Pfander B, Diffley JFX. Dpb11 coordinates Mec1 kinase activation with cell cycle-
970 regulated Rad9 recruitment. The EMBO journal. 2011;30: 4897–907.
971 doi:10.1038/emboj.2011.345

972 54. Torres-Rosell J, Mahín F, Farmer S, Jarmuz A, Eydmann T, Dalgaard JZ, et al. SMC5 and
973 SMC6 genes are required for the segregation of repetitive chromosome regions. Nature Cell
974 Biology. 2005;7: 412–419. doi:10.1038/ncb1239

975 55. Horigome C, Bustard DE, Marcomini I, Delgoshaie N, Tsai-Pflugfelder M, Cobb JA, et al.
976 PolySUMOylation by Siz2 and Mms21 triggers relocation of DNA breaks to nuclear pores
977 through the Slx5/Slx8 STUbL. Genes & Development. 2016;30: 931–945.
978 doi:10.1101/gad.277665.116

979 56. Elserafy M, El-Khamisy SF. Choose your yeast strain carefully: the RAD5 gene matters.
980 Nature Reviews Molecular Cell Biology. 2018;19: 343–344. doi:10.1038/s41580-018-
981 0005-2

982 57. Kaliraman V, Brill S. Role of SGS1 and SLX4 in maintaining rDNA structure in
983 *Saccharomyces cerevisiae*. Curr Genet. 2002;41: 389–400. doi:10.1007/s00294-002-0319-6

984 58. Zappulla DC, Maharaj ASRR, Connelly JJ, Jockusch RA, Sternglanz R. Rtt107/Esc4 binds
985 silent chromatin and DNA repair proteins using different BRCT motifs. BMC Mol Biol.
986 2006;7: 40. doi:10.1186/1471-2199-7-40

987 59. Endo K, Tago YI, Daigaku Y, Yamamoto K. Error-free RAD52 pathway and error-prone
988 REV3 pathway determines spontaneous mutagenesis in *Saccharomyces cerevisiae*. Genes
989 Genet Syst. 2007;82: 35–42. doi:10.1266/ggs.82.35

990 60. Hoege C, Pfander B, Moldovan G-L, Pyrowolakis G, Jentsch S. RAD6-dependent DNA
991 repair is linked to modification of PCNA by ubiquitin and SUMO. Nature. 2002;419: 135–
992 141. doi:10.1038/nature00991

993 61. Boiteux S, Jinks-Robertson S. DNA repair mechanisms and the bypass of DNA damage in
994 Saccharomyces cerevisiae. Genetics. 2013;193: 1025–1064.
995 doi:10.1534/genetics.112.145219

996 62. Janke R, Kong J, Braberg H, Cantin G, Yates K JR, N.J. Nonsense-mediated decay
997 regulates key components of homologous recombination. Nucleic Acids Res. 2016;44:
998 5218–5230. doi:10.1093/nar/gkw182

999 63. Srivas R, Shen JP, Yang CC, Sun SM, Li J, Gross AM. A network of conserved synthetic
1000 lethal interactions for exploration of precision cancer therapy. Mol Cell. 2016;63: 514–525.
1001 doi:10.1016/j.molcel.2016.06.022

1002 64. Ye P, Peyser BD, Pan X, Boeke JD, Spencer FA, Bader JS. Gene function prediction from
1003 congruent synthetic lethal interactions in yeast. Molecular systems biology. 2005;1:
1004 2005.0026. doi:10.1038/msb4100034

1005 65. Tong AHY, Lesage G, Bader GD, Ding H, Xu H, Xin X. Global mapping of the yeast
1006 genetic interaction network. Science. 2004;303: 808–813. doi:10.1126/science.1091317

1007 66. Kuzmin E, VanderSluis B, Wang W, Tan G, Deshpande R, Chen Y. Systematic analysis of
1008 complex genetic interactions. Science. 360: 1729. doi:10.1126/science.aao1729.

1009 67. Costanzo M, Baryshnikova A, Bellay J, Kim Y, Spear ED, Sevier CS. The genetic
1010 landscape of a cell. Science. 2010;327: 425–31. doi:10.1126/science.1180823

1011 68. Costanzo M, VanderSluis B, Koch EN, Baryshnikova A, Pons C, Tan G. A global genetic
1012 interaction network maps a wiring diagram of cellular function. Science. 2016;353: 549–
1013 562. doi:10.1126/science.aaf1420

1014 69. Tong AHY, Evangelista M, Parsons AB, Xu H, Bader GD, Pagé N. Systematic genetic
1015 analysis with ordered arrays of yeast deletion mutants. Science. 2001;294: 2364–2368.
1016 doi:10.1126/science.1065810

1017 70. Collins SR, Miller KM, Maas NL, Roguev A, Fillingham J, Chu CS, et al. Functional
1018 dissection of protein complexes involved in yeast chromosome biology using a genetic
1019 interaction map. Nature. 2007;446: 806–810. doi:10.1038/nature05649

1020 71. Pan X, Ye P, Yuan DS, Wang X, Bader JS, Boeke JD. A DNA integrity network in the
1021 yeast Saccharomyces cerevisiae. Cell. 2006;124: 1069–1081.
1022 doi:10.1016/j.cell.2005.12.036

1023 72. Styles EB, Founk KJ, Zamparo LA, Sing TL, Altintas D, Ribeyre C. Exploring quantitative
1024 yeast phenomics with single-cell analysis of DNA damage foci. Cell Syst. 2016;3: 264-277
1025 10. doi:10.1016/j.cels.2016.08.008

1026 73. Leung GP, Aristizabal MJ, Krogan NJ, Kobor MS. Conditional genetic interactions of
1027 RTT107, SLX4, and HRQ1 reveal dynamic networks upon DNA damage in S. cerevisiae.
1028 G3 (Bethesda). 2014;4: 1–33. doi:10.1534/g3.114.011205

1029 74. Hum YF, Jinks-Robertson S. DNA strand-exchange patterns associated with double-strand
1030 break-induced and spontaneous mitotic crossovers in Saccharomyces cerevisiae. PLoS
1031 Genet. 2018;14: 1–26. doi:10.1371/journal.pgen.1007302

1032 75. Lee PS, Greenwell PW, Dominska M, Gawel M, Hamilton M, Petes TD. A fine-structure
1033 map of spontaneous mitotic crossovers in the yeast Saccharomyces cerevisiae. PLOS
1034 Genetics. 2009;5: e1000410.

1035 76. Jinks-Robertson S, Petes TD. Mitotic recombination in yeast: what we know and what we
1036 don't know. Current Opinion in Genetics & Development. 2021;71: 78–85.
1037 doi:10.1016/j.gde.2021.07.002

1038 77. Wolner B, Van Komen S, Sung P, Peterson CL. Recruitment of the recombinational repair
1039 machinery to a DNA double-strand break in yeast. Mol Cell. 2003;12: 221–232.
1040 doi:10.1016/S1097-2765(03)00242-9

1041 78. Renkawitz J, Lademann CA, Kalocsay M, Jentsch S. Monitoring homology search during
1042 DNA double-strand break repair in vivo. Mol Cell. 2013;50: 261–272.
1043 doi:10.1016/j.molcel.2013.02.020

1044 79. Herzberg K, Bashkirov VI, Rolfsmeier M, Haghnazari E, McDonald WH, Anderson S, et
1045 al. Phosphorylation of Rad55 on Serines 2, 8, and 14 Is Required for Efficient Homologous
1046 Recombination in the Recovery of Stalled Replication Forks. Molecular and Cellular
1047 Biology. 2006;26: 8396–8409. doi:10.1128/MCB.01317-06

1048 80. Roy U, Greene EC. The Role of the Rad55–Rad57 Complex in DNA Repair. Genes.
1049 2021;12: 1390. doi:10.3390/genes12091390

1050 81. Li F, Dong J, Pan X, Oum JH, Boeke JD, Lee SE. Microarray-based genetic screen defines
1051 SAW1, a gene required for Rad1/Rad10-dependent processing of recombination
1052 intermediates. Mol Cell. 2008;30: 325–335. doi:10.1016/j.molcel.2008.02.028

1053 82. Rozenzhak S, Mejía-Ramírez E, Williams JS, Schaffer L, Hammond JA, Head S. Rad3ATR
1054 decorates critical chromosomal domains with γH2A to protect genome integrity during S-
1055 phase in fission yeast. PLoS Genet. 2010;6: 1–17. doi:10.1371/journal.pgen.1001032

1056 83. Williams JS, Williams RS, Dovey CL, Guenther G, Tainer J a, Russell P. gammaH2A binds
1057 Brc1 to maintain genome integrity during S-phase. The EMBO journal. 2010;29: 1136–
1058 1148. doi:10.1038/emboj.2009.413

1059 84. Javaheri A, Wysocki R, Jobin-Robitaille O, Altaf M, Côté J, Kron SJ. Yeast G1 DNA
1060 damage checkpoint regulation by H2A phosphorylation is independent of chromatin
1061 remodeling. Proceedings of the National Academy of Sciences of the United States of
1062 America. 2006;103: 13771–6. doi:10.1073/pnas.0511192103

1063 85. Giannattasio M, Lazzaro F, Plevani P, Muzi-Falconi M. The DNA damage checkpoint
1064 response requires histone H2B ubiquitination by Rad6-Bre1 and H3 methylation by Dot1.
1065 The Journal of biological chemistry. 2005;280: 9879–86. doi:10.1074/jbc.M414453200

1066 86. Grenon M, Costelloe T, Jimeno S, Shaughnessy AO, Fitzgerald J, Zgheib O, et al. Docking
1067 onto chromatin via the Saccharomyces cerevisiae Rad9 Tudor domain. 2007; 105–119.
1068 doi:10.1002/yea

1069 87. Wysocki R, Javaheri A, Allard S, Sha F, Côté J, Kron SJ, et al. Role of Dot1-Dependent
1070 Histone H3 Methylation in G 1 and S Phase DNA Damage Checkpoint Functions of Rad9.
1071 2005. doi:10.1128/MCB.25.19.8430

1072 88. Zaidi IW, Rabut G, Poveda A, Scheel H, Malmström J, Ulrich H, et al. Rtt101 and Mms1 in
1073 budding yeast form a CUL4 DDB1 -like ubiquitin ligase that promotes replication through
1074 damaged DNA. EMBO Rep. 2008;9: 1034–1040. doi:10.1038/embor.2008.155

1075 89. Sikorski RS, Hieter P. A system of shuttle vectors and yeast host strains designed for
1076 efficient manipulation of DNA in Saccharomyces cerevisiae. Genetics. 1989;122: 19–27.
1077 doi:10.1093/genetics/122.1.19

1078 90. Moore JD, Yazgan O, Ataian Y, Krebs JE. Diverse roles for histone H2A modifications in
1079 DNA damage response pathways in yeast. Genetics. 2007;176: 15–25.
1080 doi:10.1534/genetics.106.063792

1081 **Supplementary Figure Captions**

1082 **Fig. S1. Rtt107 did not limit spontaneous LOH by regulating the Rad9–Dpb11 interaction.**

1083 The *rad9-2A* allele enhanced the spontaneous LOH rate of the *rtt107*Δ mutant in the bimater
1084 assay. Mating rates were calculated and compared as described for the bimater assay in Figure
1085 2B. +, non-overlap of 95% confidence intervals between two strains (statistically significant); ns,
1086 overlap of confidence intervals (not significant). This experiment was performed in the W303
1087 *rad5-535* background, and 12 independent colonies were tested.

1088 **Fig. S2. Rtt107 limited rDNA recombination in the same pathway as Slx4.**

1089 The *rtt107*Δ, *slx4*Δ, and *rtt107*Δ *slx4*Δ mutants exhibited similar rDNA hyperrecombination
1090 phenotypes. rDNA recombination rates and 95% confidence intervals were determined as
1091 described in Figure 4D. +, non-overlap of 95% confidence intervals between two strains
1092 (statistically significant); ns, overlap of confidence intervals (not significant). This experiment
1093 was performed in the W303 *RAD5* background, and eight independent colonies were tested.

1094 **Fig. S3. Rtt107 did not primarily limit spontaneous LOH by regulating DNA damage**
1095 **tolerance pathways.**

1096 Deletion of *UBC13* did not affect the rate of LOH in the wild-type or *rtt107*Δ mutant. Mating
1097 rates were calculated and compared as described for the bimater assay in Figure 2B. +, non-
1098 overlap of 95% confidence intervals between two strains (statistically significant); ns, overlap of
1099 confidence intervals (not significant). This experiment was performed in the W303 *rad5-535*
1100 background, and 11-12 independent colonies were tested.

1101 **Fig. S4. The *rad55-S404A* mutation did not affect Rad55 protein level.**

1102 Immunoblotting was performed using anti-FLAG antibody on whole-cell extract. Anti-PGK1
1103 antibody was used as a loading control.

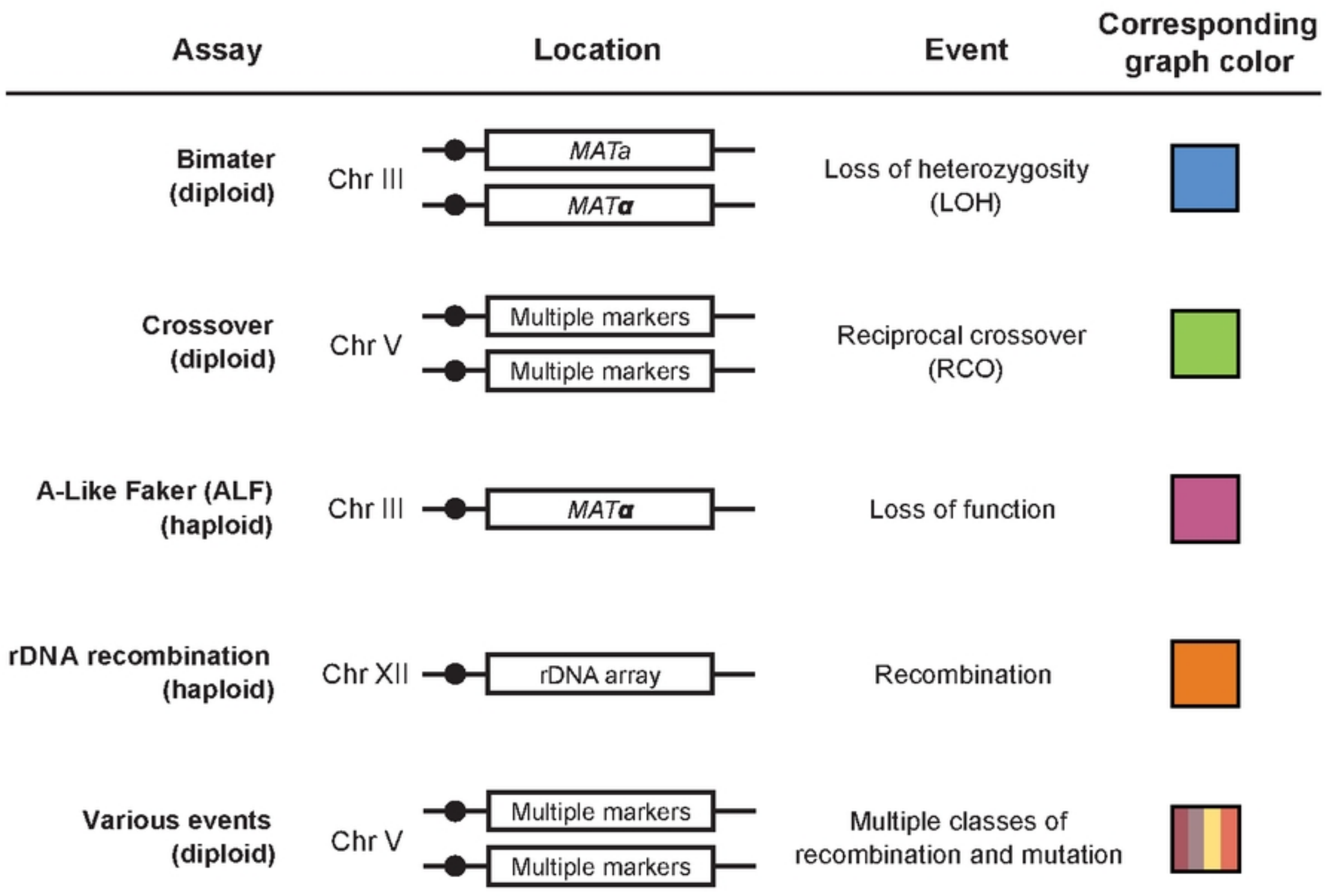
Assay
Location
Event
Corresponding graph color
Bimater (diploid)
Chr III
MATa
MATα
Loss of heterozygosity (LOH)
Crossover (diploid)
Chr V
Multiple markers
Multiple markers
Reciprocal crossover (RCO)
A-Like Faker (ALF) (haploid)
Chr III
MATα
Loss of function
rDNA recombination (haploid)
Chr XII
rDNA array
Recombination
Various events (diploid)
Chr V
Multiple markers
Multiple markers
Multiple classes of recombination and mutation

Fig. 1.

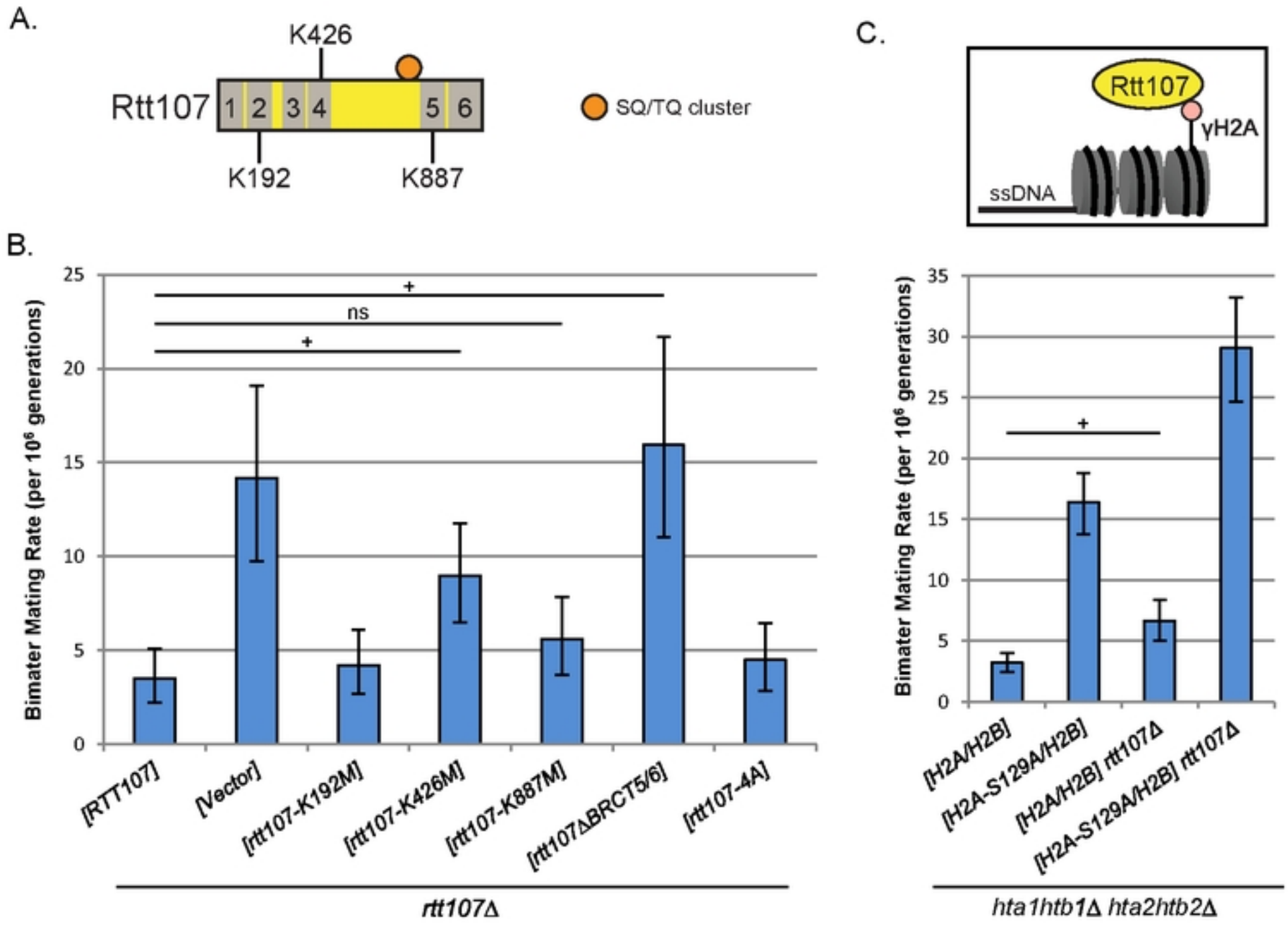
A.
K426
Rtt107
1 2 3 4 5 6
K192
K887
SQ/TQ cluster
B.
Bimater Mating Rate (per 10^6 generations)
25
20
15
10
5
0
+
ns
+
[RTT107]
[Vector]
[rtt107-K192M]
[rtt107-K426M]
[rtt107-K887M]
[rtt107ΔBRCT5/6]
[rtt107-4A]
rtt107Δ
C.
Rtt107
γH2A
ssDNA
Bimater Mating Rate (per 10^6 generations)
35
30
25
20
15
10
5
0
+
[H2A/H2B]
[H2A-S129A/H2B]
[H2A/H2B] rtt107Δ
[H2A-S129A/H2B] rtt107Δ
hta1htb1Δ hta2htb2Δ

Fig. 2.

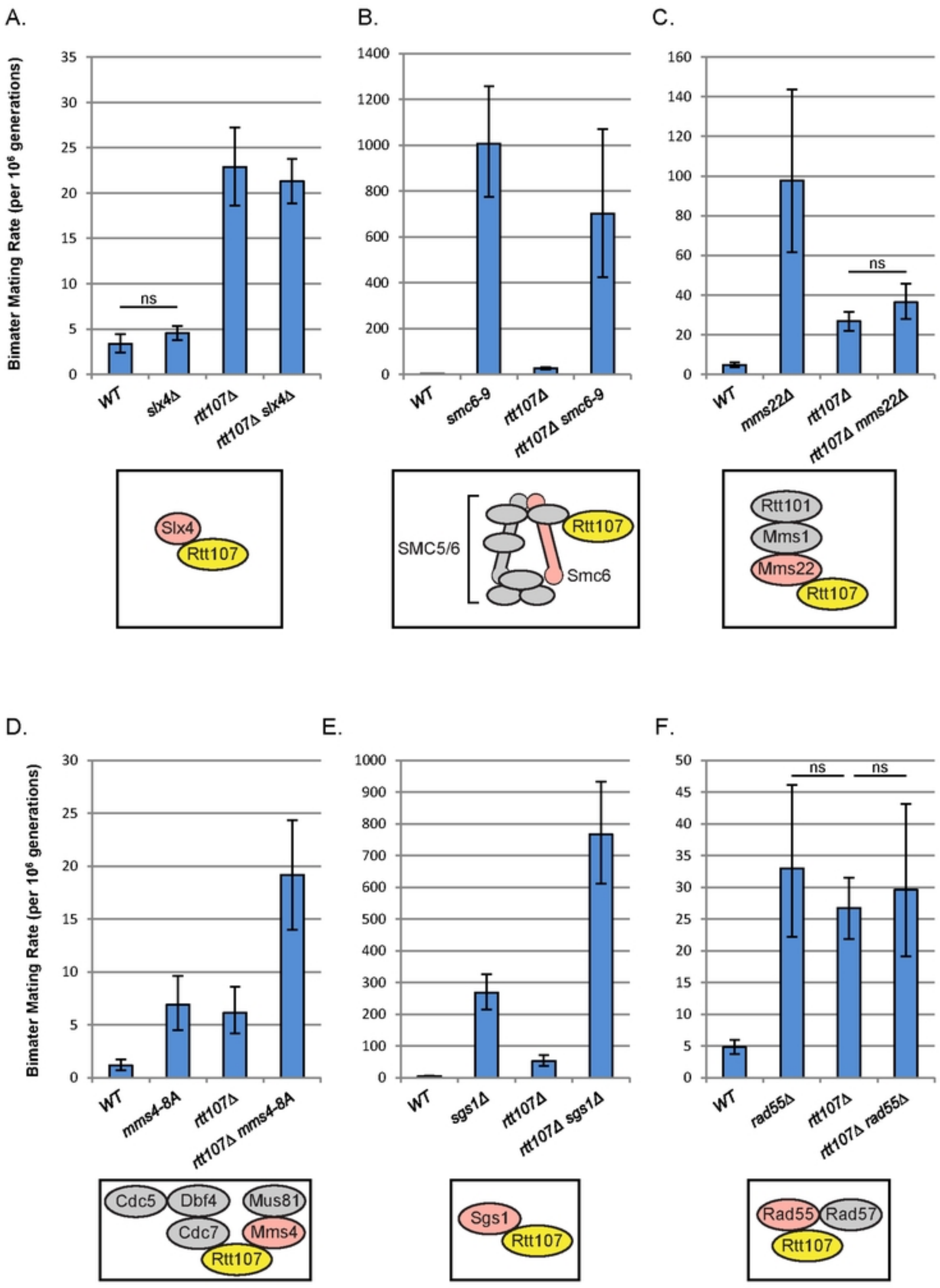
A.
B.
C.
D.
E.
F.
Bimater Mating Rate (per 10⁶ generations)
ns
WT
slx4Δ
rtt107Δ
rtt107Δ slx4Δ
smc6-9
rtt107Δ smc6-9
mms22Δ
rtt107Δ mms22Δ
mms4-8A
rtt107Δ mms4-8A
sgs1Δ
rtt107Δ sgs1Δ
rad55Δ
rtt107Δ rad55Δ
Slx4
Rtt107
SMC5/6
Smc6
Rtt101
Mms1
Mms22
Cdc5
Dbf4
Mus81
Cdc7
Mms4
Sgs1
Rad55
Rad57

Fig. 3.

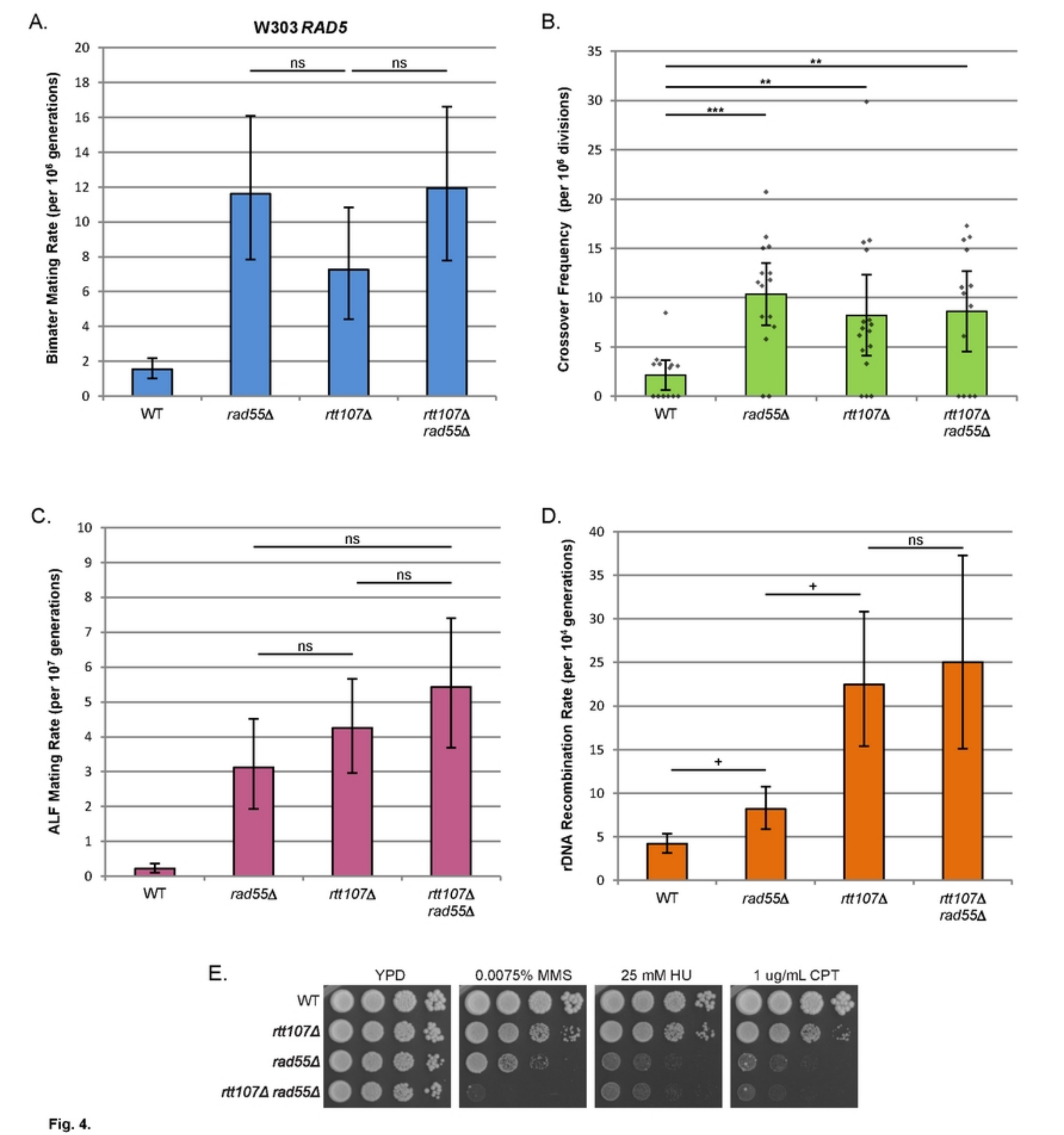
A.
W303 RAD5
Bimater Mating Rate (per 10^6 generations)
ns
ns
WT
rad55Δ
rtt107Δ
rtt107Δ rad55Δ
B.
Crossover Frequency (per 10^6 divisions)
**
**
***
WT
rad55Δ
rtt107Δ
rtt107Δ rad55Δ
C.
ALF Mating Rate (per 10^7 generations)
ns
ns
ns
WT
rad55Δ
rtt107Δ
rtt107Δ rad55Δ
D.
rDNA Recombination Rate (per 10^4 generations)
ns
+
+
WT
rad55Δ
rtt107Δ
rtt107Δ rad55Δ
E.
YPD
0.0075% MMS
25 mM HU
1 ug/mL CPT
WT
rtt107Δ
rad55Δ
rtt107Δ rad55Δ

Fig. 4.

A.

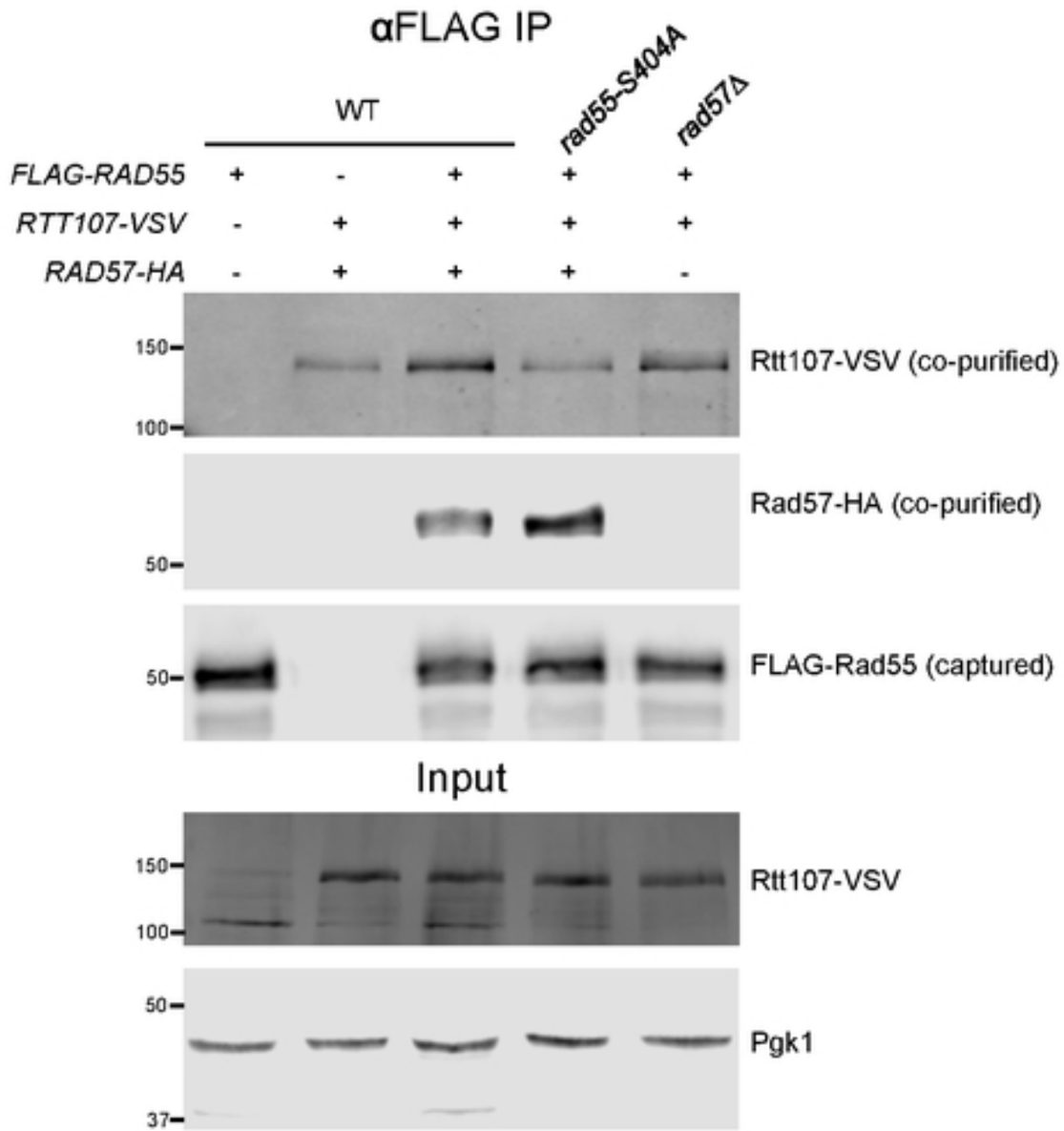
αFLAG IP
WT
rad55-S404A
rad57Δ
FLAG-RAD55 + - + + +
RTT107-VSV - + + + +
RAD57-HA - + + + -
150
100
Rtt107-VSV (co-purified)
50
Rad57-HA (co-purified)
50
FLAG-Rad55 (captured)
Input
150
100
Rtt107-VSV
50
Pgk1
37

B.

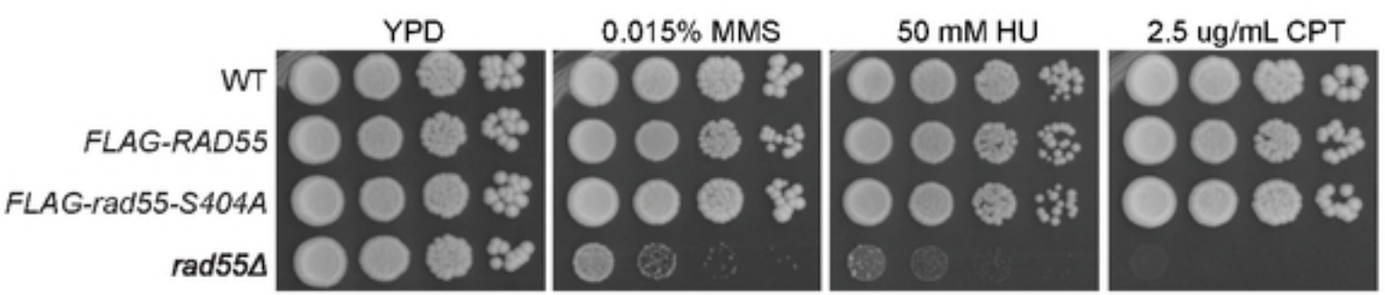
YPD
0.015% MMS
50 mM HU
2.5 ug/mL CPT
WT
FLAG-RAD55
FLAG-rad55-S404A
rad55Δ

Fig. 5.

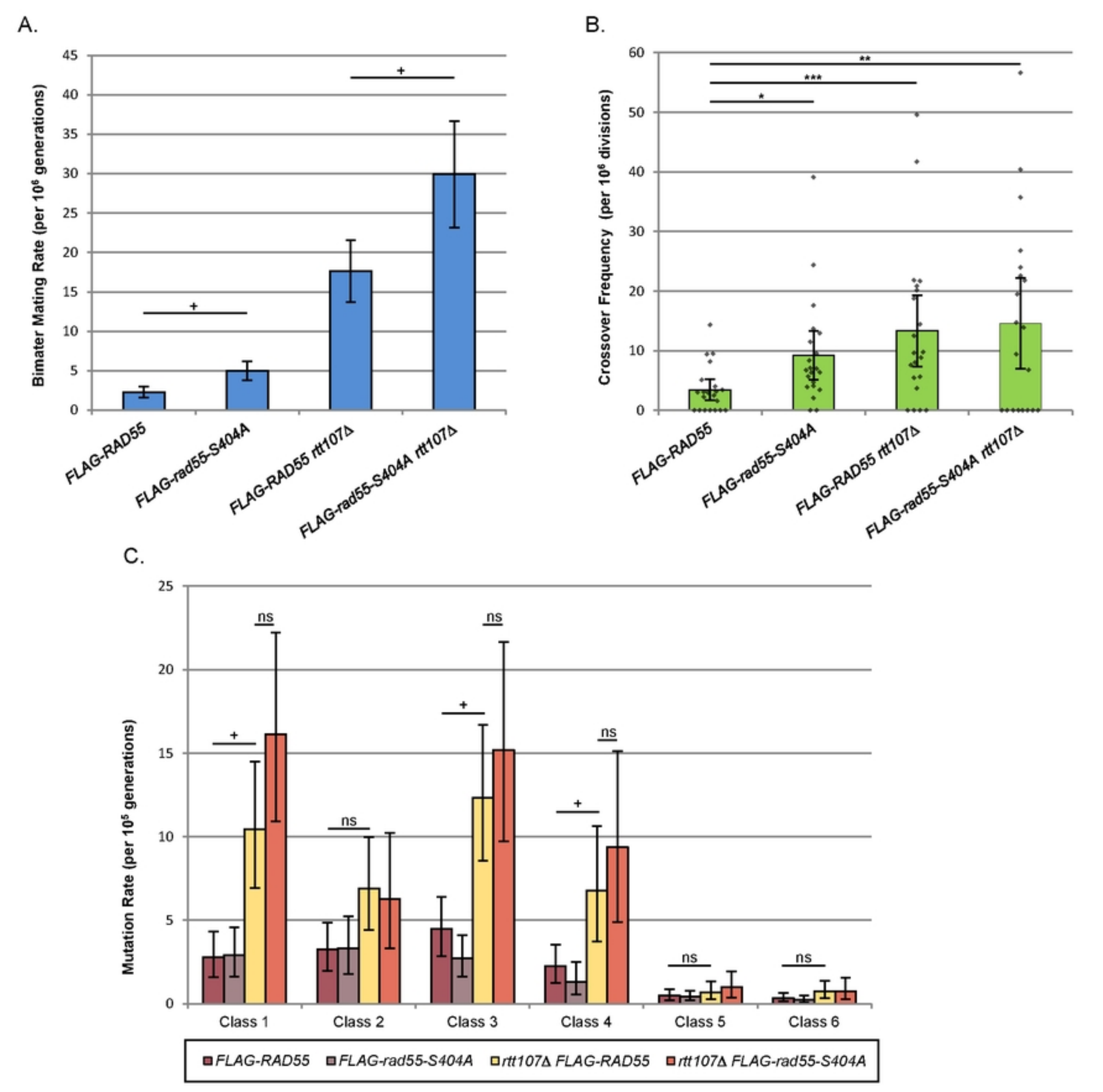
A.
Bimater Mating Rate (per 10⁶ generations)
45
40
35
30
25
20
15
10
5
0
+
+
FLAG-RAD55
FLAG-rad55-S404A
FLAG-RAD55 rtt107Δ
FLAG-rad55-S404A rtt107Δ
B.
Crossover Frequency (per 10⁶ divisions)
60
50
40
30
20
10
0
**
***
*
FLAG-RAD55
FLAG-rad55-S404A
FLAG-RAD55 rtt107Δ
FLAG-rad55-S404A rtt107Δ
C.
Mutation Rate (per 10⁵ generations)
25
20
15
10
5
0
ns
ns
+
+
ns
ns
+
ns
ns
Class 1
Class 2
Class 3
Class 4
Class 5
Class 6
FLAG-RAD55
FLAG-rad55-S404A
rtt107Δ FLAG-RAD55
rtt107Δ FLAG-rad55-S404A

Fig. 6.

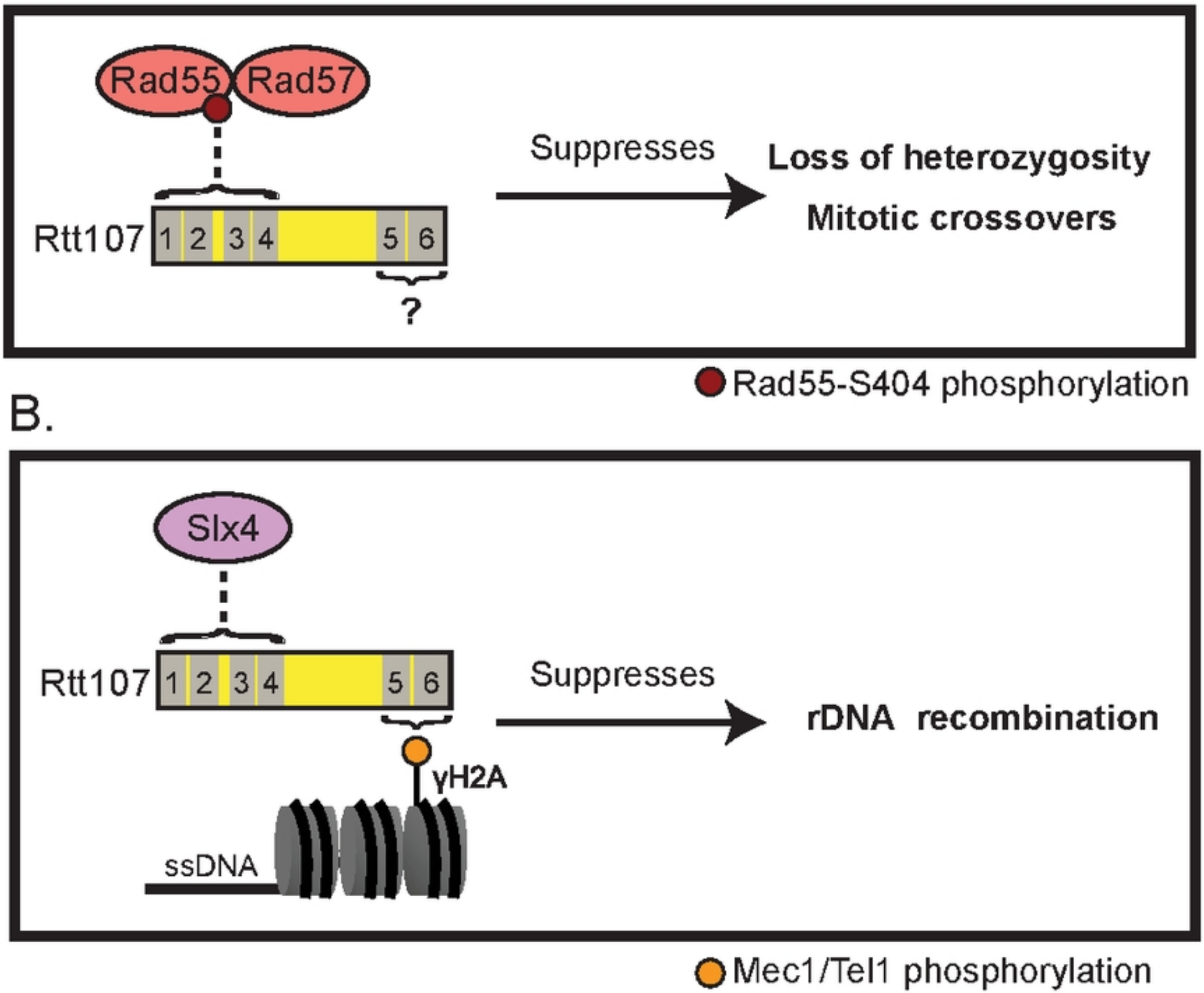
A.
Rad55
Rad57
Rtt107
1
2
3
4
5
6
?
Suppresses
Loss of heterozygosity
Mitotic crossovers
Rad55-S404 phosphorylation
B.
Slx4
Rtt107
1
2
3
4
5
6
γH2A
ssDNA
Suppresses
rDNA recombination
Mec1/Tel1 phosphorylation

Fig. 7.